INFORMATION TO USERS

This was produced from a copy of a document sent to us for microfilming. While the most advanced technological means to photograph and reproduce this document have been used, the quality is heavily dependent upon the quality of the material submitted.

The following explanation of techniques is provided to help you understand markings or notations which may appear on this reproduction.

1. The sign or "target" for pages apparently lacking from the document photographed is "Missing Page(s)". If it was possible to obtain the missing page(s) or section, they are spliced into the film along with adjacent pages. This may have necessitated cutting through an image and duplicating adjacent pages to assure you of complete continuity.

2. When an image on the film is obliterated with a round black mark it is an indication that the film inspector noticed either blurred copy because of movement during exposure, or duplicate copy. Unless we meant to delete copyrighted materials that should not have been filmed, you will find a good image of the page in the adjacent frame.

3. When a map, drawing or chart, etc., is part of the material being photographed the photographer has followed a definite method in "sectioning" the material. It is customary to begin filming at the upper left hand corner of a large sheet and to continue from left to right in equal sections with small overlaps. If necessary, sectioning is continued again—beginning below the first row and continuing on until complete.

4. For any illustrations that cannot be reproduced satisfactorily by xerography, photographic prints can be purchased at additional cost and tipped into your xerographic copy. Requests can be made to our Dissertations Customer Services Department.

5. Some pages in any document may have indistinct print. In all cases we have filmed the best available copy.

University
Microfilms
International

300 N. ZEEB ROAD, ANN ARBOR, MI 48106
18 BEDFORD ROW, LONDON WC1R 4EJ, ENGLAND

FENSTERMACHER, PHILIP RANDOLPH

LASER DOPPLER VELOCIMETRY STUDY OF THE ONSET OF CHAOS IN TAYLOR VORTEX FLOW

City University of New York PH.D. 1980

PLEASE NOTE:

In all cases this material has been filmed in the best possible way from the available copy. Problems encountered with this document have been identified here with a check mark ✓.

1. Glossy photographs _____
2. Colored illustrations _____
3. Photographs with dark background _____
4. Illustrations are poor copy ✓
5. Print shows through as there is text on both sides of page _____
6. Indistinct, broken or small print on several pages ✓
7. Tightly bound copy with print lost in spine _____
8. Computer printout pages with indistinct print _____
9. Page(s) _____ lacking when material received, and not available from school or author
10. Page(s) _____ seem to be missing in numbering only as text follows
11. Poor carbon copy _____
12. Not original copy, several pages with blurred type _____
13. Appendix pages are poor copy _____
14. Original copy with light type _____
15. Curling and wrinkled pages _____
16. Other _____

University Microfilms International

300 N. ZEEB RD., ANN ARBOR, MI 48106 (313) 761-4700

LASER DOPPLER VELOCIMETRY STUDY OF THE ONSET OF CHAOS IN TAYLOR VORTEX FLOW

BY

P. R. FENSTERMACHER

A dissertation submitted to the Graduate Faculty in Physics in partial fulfillment of the requirements for the degree of Doctor of Philosophy, The City University of New York.

1980

This manuscript has been read and accepted for the Graduate Faculty in Physics in satisfaction of the dissertation requirement for the degree of Doctor of Philosophy.

5/23/79
date

Harry L Swinney
Chairman of the Examining Committee

2/26/80
date

Grant Mathias
Executive Officer

C. Grimes
Jerry Gollub
C. M. Tchen
Supervisory Committee

The City University of New York

ABSTRACT

The Laser Doppler Velocimetry technique was used to study the mechanism by which chaos can appear in a system governed by deterministic equations of motion and time-independent boundary conditions. Incompressible fluid flow between concentric cylinders, induced by the rotation of the inner one with the outer one fixed, was chosen because it displays a progression of instabilities with increasing Reynolds number before the onset of chaos. Early workers[1] thought the number of instabilities so large that the flow appears chaotic when it is actually highly multiply-periodic. Recent work[2] cast doubt on this picture. The present study used a mini- computer on line to a PDP-10 mainframe to acquire long data records. The computed velocity power spectral densities therefore had a resolution of (10^{-4}). High optical mixing efficiency provided a signal to noise ratio three orders of magnitude higher than previous studies. As a result, we have been able to precisely characterize a quasi-periodic flow and show that chaos appears after two time-dependent instabilities. Relationships of the mode frequencies at the onset of chaos are examined.

References

1. Landau, L. 1944 "On the problem of turbulence." C.R. (Dokl.) Acad. Sci. URSS 44, 311-315.

2. Gollub, J.P. and Swinney, H.L. 1975 "Onset of turbulence in a rotating fluid." Phys. Rev. Lett. 35, 927-930.

ACKNOWLEDGEMENTS

With so many to thank for so much, I won't try to do full justice, but confine myself to the highlights. My advisor, Professor Harry L. Swinney; at times worked side by side with me, taught me the important art of the presentation of knowledge, and shared a bunch of Super Crunch. My co-advisor, Professor J. P. Gollub was instrumental in the formulation of the problem and getting the initial work off the ground. Distinguished Professor Herman Z. Cummins, who headed the Light Scattering Laboratory, set an example for us all. He really is distinguished.

Many colleagues made the passage a little easier. Some were scientific older brothers like Dr. Richard Leigh and Dr. James Haddad. Some passed the whole route with me like Dr. Apostolos Doukas and Dr. Jenn-Shyong Hwang. Most especially, Dr. Dennis Wonica revived me when I was sure I had nothing left.

Many people contribute to the research effort at City College, but sadly don't often share the rewards. Mr. George Kleiner, director of the Computer Center, was always willing to give a little extra to make things possible. No experiment can be done without skilled craftsmen who can make a new scientific instrument from an idea and a block of steel. I thank all the gentlemen of the shop and especially Mr. Robert Quinlan, Mr. Robert Cope, Mr. Jerry Cannella, Mr. Archie Nucatola, and Mr. Marty Whitman. Secretaries are the secret force that really run any organization. Mrs. Bertha Danziger is the force of the Physics Department and Mrs. Frances Tritt is the force of the Light Scattering Laboratory. And Mr. Benjamin Jordan helped me through the hour of the wolf.

Another bunch of people have kept the CUNY Graduate Center from becoming a Mac Donald's. Mrs. Bea Rosenberg of the Bursar's Office and Mr. Gustavo Archilla of the Registrar's Office did just a little bending of the rules to make up for my not too infrequent irresponsibility. Mrs. Florence Brill, past secretary of the Physics program, did the same and gave me the most rousing pep talks. Mrs. Rose Chafetz is carrying on the tradition for a new generation of graduate students.

Research is an assured deterrent to social life. Lovers and friends are lost, but a few remain. My roomate, Mr. Beriau Picard, jocularly pointed out that part of my degree belongs to him. He's right. Another piece goes to Mr. LeRoy Baxter and his wife Marie-Noelle who understand friendship in the European way. And of course, a piece goes to Mom. I get a card on every known and some unknown holidays.

TABLE OF CONTENTS

LIST OF TABLES

LIST OF FIGURES

1. INTRODUCTION

Turbulent flows are the rule rather than the exception in nature, but our understanding of fluid flows is predominately of the laminar case. In turbulence theory most of the attention has been given to the fully developed case and relatively little to its onset. The theories of fully developed turbulence introduce a statistical description ad hoc, an approach which assumes that a very large number of modes of the fluid are excited. In the transition problem, we are attempting to understand what modes are involved and how they become excited. The current study supports the view that the number of modes involved in the appearance of turbulence need not be large.

The flow between concentric rotating cylinders is a natural choice as a system for study because its high symmetry has made the study of the laminar regimes very successful compared to more general flows. However, as we shall see in what follows, a great deal remains unknown in this system. It is unlikely that a deeper understanding of the transition problem will come first from a more general flow. Similarly, in the hope of obtaining deeper insight by restricting the problem, we have chosen the case of the outer cylinder at rest with the inner cylinder rotating. This restriction represents a modest experimental convenience, but the main reason for this choice is the apparent difference in the character of the transition to turbulence

in this case as compared to the case where motion of the outer cylinder predominates. In the later case turbulence can appear directly and catastrophically from Taylor vortex flow[1]. In the case we have studied, intermediate states were known to occur before the appearance of turbulence, but the present study shows that their number can be reduced by using short cylinders. This study also shows that additional previously unknown instabilities occur. The hope is that the study of this progression will lead to insight into the onset of turbulence.

In Chapter 2 we review previous work on this progression of flows. In Chapter 3 we describe the principles of laser Doppler velocimetry pertinent to our work. In Chapter 4 we describe the flow apparatus in which our measurements were made and the laser Doppler velocimetry technique used. In Chapter 5 we present our results. The implications and conclusions that can be drawn from these results are presented in Chapters 6 and 7.

Reference for Chapter I

1. Coles, D. 1965 Transition in Circular Couette flow. J. Fluid Mech. 21, 385-425.

2. REVIEW

2.1. Groundwork

Theoretical approaches reviewed here generally assume that a fluid dynamic description is rich enough to describe the phenomena. The experimental results are generally not bound by this assumption and often serve to justify it. It is further assumed that a viscous fluid must locally match the velocity of a solid boundary. This assumption has been justified theoretically by examining a thin layer near the boundary in an expanded coordinate system and allowing the fluid to slip at the boundary. It is found that for very small boundary surface irregularities a surface of fluid velocity equal to that of the boundary exists very near to the boundary[1]. Finally, it is assumed that the fluid is incompressible. This assumption is justified if the molecular relaxation of density gradients is rapid compared to the characteristic time scales of the fluid motion. A measure of the rate of equalization of density gradients is the sound speed, and the desired parameter expressing the incompressibility of the flow is the ratio of the fluid velocity to the sound speed, which for our system is always less than 10^{-3}. Despite these restrictions, and half a century of effort, the resulting theoretical model is still largely unexplored. Thus it is reasonable to explore this model further before considering something more general.

The previous considerations result in the Navier-Stokes

equation as the equation of motion of the system:

$$\frac{\partial \vec{v}}{\partial t} + (\vec{v}\cdot\nabla)\vec{v} = -\nabla p + \frac{1}{R}\nabla^2\vec{v} \qquad (2.1)$$

in dimensionless units where:

$$R = \frac{UL}{\nu} \qquad (2.2)$$

and U is the scale velocity, L the scale length, and ν the kinematic viscosity. The continuity equation:

$$\vec{\nabla}\cdot\vec{v} = 0 \qquad (2.3)$$

is also part of the system of governing equations, but it should be noted that use has already been made of it in the form of the viscosity(last) term of (2.1) and in some cases it yields no new information. For the case of concentric cylinders the natural representation of (2.1) and (2.3) is cylindrical coordinates with axes chosen as shown in figure 2.1 and u,v,w are the components of v in the r, ϕ, and z directions, respectively.

$$\begin{aligned}
&\frac{\partial u}{\partial t} + u\frac{\partial u}{\partial r} + \frac{v}{r}\frac{\partial u}{\partial \phi} + w\frac{\partial u}{\partial z} - \frac{v^2}{r} = -\frac{\partial p}{\partial r} + \frac{1}{R}\left(\nabla^2 u - \frac{u}{r^2} - \frac{2}{r^2}\frac{\partial v}{\partial \phi}\right)\\
&\frac{\partial v}{\partial t} + u\frac{\partial v}{\partial r} + \frac{v}{r}\frac{\partial v}{\partial \phi} + w\frac{\partial v}{\partial z} - \frac{uv}{r} = -\frac{1}{r}\frac{\partial p}{\partial \phi} + \frac{1}{R}\left(\nabla^2 v - \frac{v}{r^2} + \frac{2}{r^2}\frac{\partial u}{\partial \phi}\right)\\
&\frac{\partial w}{\partial t} + u\frac{\partial w}{\partial r} + \frac{v}{r}\frac{\partial w}{\partial \phi} + w\frac{\partial w}{\partial z} = -\frac{\partial p}{\partial z} + \frac{1}{R}\nabla^2 w\\
&\frac{1}{r}\frac{\partial}{\partial r}(ru) + \frac{1}{r}\frac{\partial v}{\partial \phi} + \frac{\partial w}{\partial z} = 0
\end{aligned} \qquad (2.4)$$

We shall review previous work by examining the successive regimes exhibited by the flow in order of increasing Reynolds number. Our review will not be

Figure 2.1

The flow geometry with definition of the cylindrical coordinate directions and the mechanical parameters; a the innner cylinder radius, b the outer cylinder radius, c the gap width, and L the fluid height.

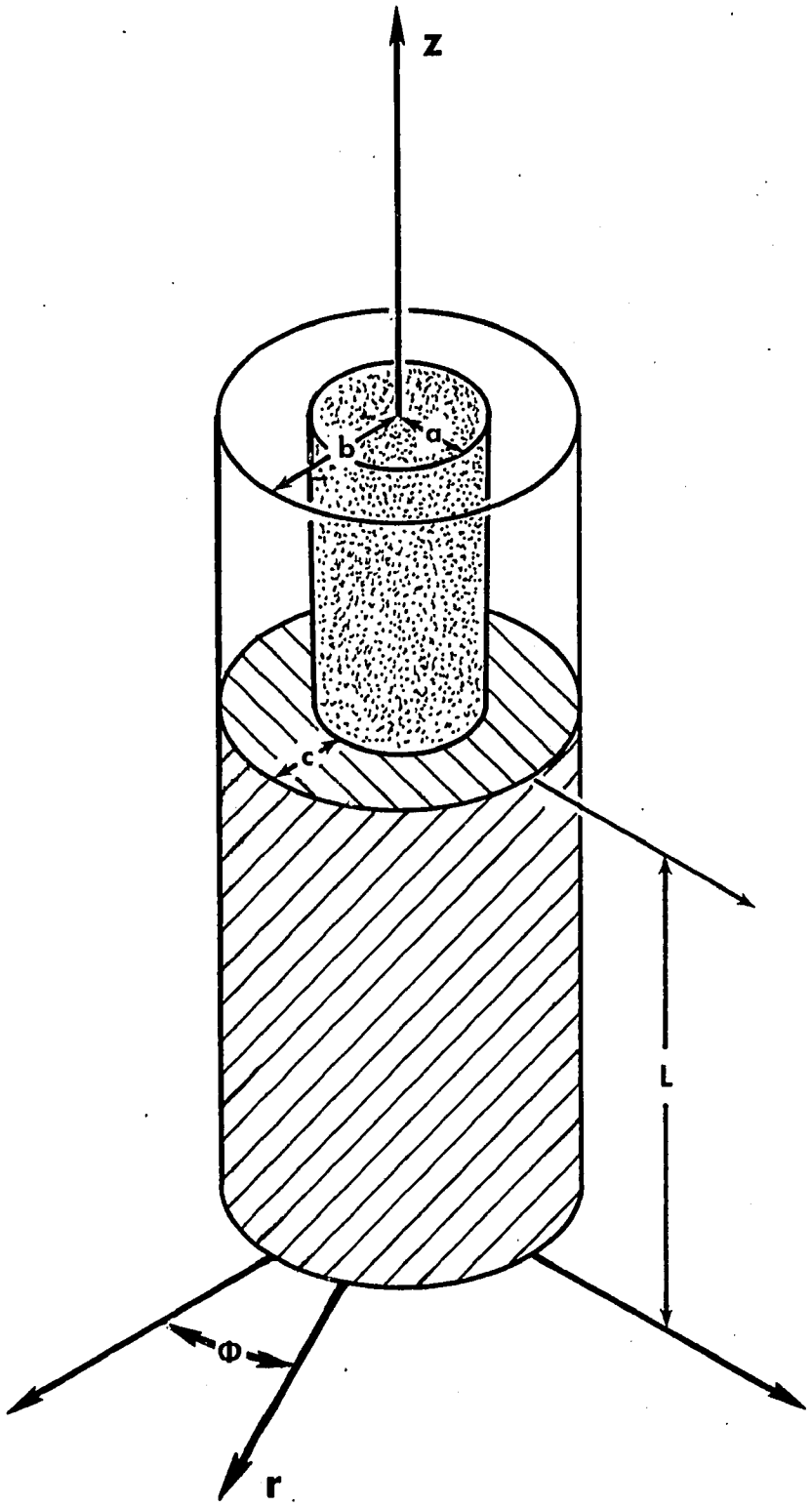
z
a
b
c
L
Φ
r

strictly historical. The flows are classified by results of theoretical work assuming infinitely long cylinders and experiments in long apparatii, but we will in each case discuss finite length results.

2.2. Couette Flow

At low Reynolds number the flow is time-independent having only a single non-vanishing velocity component in the azimuthal direction which depends only on the radial coordinate. This result can be sucessfully compared with the solution obtained from the Navier-Stokes equation by assuming that the flow shares the symmetry of the boundary conditions in the idealized case of infinite cylinders. This was done by Couette[2] as a check on the Newtonian stress approximation. The cylindrical symmetry gives:

$$\frac{\partial u}{\partial \phi} = \frac{\partial v}{\partial \phi} = \frac{\partial w}{\partial \phi} = 0 \qquad (2.5)$$

while assuming the cylinders fixed in the z-direction gives:

$$w = \frac{\partial u}{\partial z} = \frac{\partial v}{\partial z} = 0 \qquad (2.6)$$

Further, no-slip boundary conditions give $\vec{v} = (0, \Omega_1 a, 0)$ at the inner cylinder wall if it has an angular velocity of Ω_1 and $\vec{v} = (0, \Omega_2 b, 0)$ at the outer cylinder wall if it has an angular velocity of Ω_2. The normal component of this condition is held to be true in the body of the fluid. We are left with the functional form of the velocity $\vec{v} = \hat{\phi} v(r)$. Using (2.5) and (2.6) and seeking a time- independent solution so that time derivatives may be set to zero, we obtain from (2.4):

$$\frac{d^2v}{dr^2} + \frac{1}{r}\frac{dv}{dr} - \frac{v}{r^2} = 0$$

$$\frac{dp}{dr} = \frac{v^2}{r} \qquad (2.7)$$

Note that this system is linear, the first of which has the solution:

$$v = Ar + \frac{B}{r} \qquad (2.8)$$

where:

$$A = -\Omega_1 \eta^2 \frac{1-\mu/\eta^2}{1-\eta^2} \quad \text{and} \quad B = \frac{a^2(1-\mu)}{1-\eta^2} \qquad (2.9)$$

and:

$$\mu = \frac{\Omega_1}{\Omega_2} \quad \text{and} \quad \eta = \frac{a}{b} \qquad (2.10)$$

are determined by the boundary conditions. Note that the Reynolds number does not appear. This solution is valid for all values of the Reynolds number. This does not mean, however, that the flow it represents is observed at all Reynolds numbers. Couette and other early researchers [3] observed that this flow did not persist as the Reynolds number was increased.

2.3. Taylor Vortex flow

Rayleigh[4] presented an incisive heuristic analysis of the stability of Couette flow against axisymmetric disturbances neglecting the effect of viscosity. In this case, due to Kelvin's theorem, the angular momentum of a fluid element would remain unchanged even when displaced from its equilibrium position to a region of different angular momentum. Motion in the axial and radial directions is governed by the centrifugal force $\propto v^2/r$. Since $vr=k$, a constant, the centrifugal force is k^2/r^3 and associated with it is a potential $\rho k^2/2r^2$. The flow is stable if this potential is a minimum. To achieve that, it is necessary to have larger values of k^2 at larger radii. Thus the squared circulation must increase monotonically outward for stability.

Von Karman[5] arrived at the same criterion by considering the balance between the centrifugal force $\rho v^2/r$ and the pressure gradient. If a ring of fluid at radius r_1 is displaced to a larger radius r_2 the centrifugal force becomes:

$$\rho\left(\frac{r_1 v_1}{r_2}\right)^2/r_2 = \frac{(r_1 v_1)^2}{r_2^3} \qquad (2.11)$$

The pressure gradient at r_2 is that needed to balance the centrifugal force of the fluid originally there, $\rho v_2^2/r^2$. If the centrifual force of the newly arrived fluid is larger than the pressure gradient, there will be an unbalanced outward force which will cause the displaced fluid to

continue its motion rendering the basic flow unstable. The comparison of these two forces reduces to:

$$(r_1 v_1)^2 > (r_2 v_2)^2 \quad \text{or} \quad k_1^2 > k_2^2 \tag{2.12}$$

A similar examination of a ring of fluid at r_2 displaced to r_1 under the same circumstances shows that it experiences an unbalanced force inward. Thus when the Rayleigh criterion is not met a fluid element is unstable with respect to displacement in either radial direction. Synge[6] derived this criterion by a linear stability analysis of the inviscid equations of motion for axisymmetric disturbances and Chandrasekhar[7] demonstrated the general case. Application of the Rayleigh criterion to the case of the outer cylinder fixed indicates instability at infinitesimal Reynolds number while a finite stable regime is observed experimentally. The Rayleigh analysis must not be complete.

To include the effect of viscosity G.I. Taylor[8] performed a linear stability analysis of the Couette flow solution. Substituting:

$$\begin{aligned} u &= u' \\ v &= V + v' \\ w &= w' \end{aligned} \tag{2.13}$$

where V is given by (2.8), into (2.4) gives the equations for the time evolution of the disturbance:

$$\frac{\partial u'}{\partial t} + \frac{V}{r}\frac{\partial u'}{\partial \phi} - \frac{2V}{r}v' = -\frac{\partial p'}{\partial r} + \frac{1}{R}\left(\nabla^2 u' - \frac{u'}{r^2} - \frac{2}{r^2}\frac{\partial v'}{\partial \phi}\right)$$

$$\frac{\partial v'}{\partial t} + \frac{V}{r}\frac{\partial v'}{\partial \phi} + u'\frac{dV}{dr} + \frac{u'V}{r} = -\frac{1}{r}\frac{\partial p'}{\partial \phi} + \frac{1}{R}\left(\nabla^2 v' - \frac{v'}{r^2} + \frac{2}{r^2}\frac{\partial u'}{\partial \phi}\right)$$

$$\frac{\partial w'}{\partial t} + \frac{V}{r}\frac{\partial w'}{\partial \phi} = -\frac{\partial p'}{\partial z} + \frac{1}{R}\nabla^2 w' \qquad (2.14)$$

$$\frac{1}{r}\frac{\partial}{\partial r}(ru') + \frac{1}{r}\frac{\partial v'}{\partial \phi} + \frac{\partial w'}{\partial z} = 0$$

with boundary conditions:

$$u' = v' = w' = 0 \quad \text{for} \quad \begin{matrix} r = 1 \\ r = \frac{b}{a} \end{matrix} \qquad (2.15)$$

To investigate the evolution of axisymmetric disturbances a solution of the form:

$$\begin{aligned} u' &= \hat{u}(r)\cos\lambda z\, e^{\sigma t} \\ v' &= \hat{v}(r)\cos\lambda z\, e^{\sigma t} \\ w' &= \hat{w}(r)\sin\lambda z\, e^{\sigma t} \end{aligned} \qquad (2.16)$$

is assumed. This leads to:

$$\begin{aligned} (L - \lambda^2 - \sigma R)(L - \lambda^2)u &= 2\lambda^2 R\hat{w}v \\ (L - \lambda^2 - \sigma R)v &= 2RA\hat{u} \end{aligned} \qquad (2.17)$$

$$L = \frac{d^2}{dr^2} + \frac{1}{r}\frac{d}{dr} - \frac{1}{r^2} = \frac{d}{dr}\left(\frac{d}{dr} + \frac{1}{r}\right) \qquad (2.18)$$

with boundary conditions:

$$\hat{u} = \frac{d\hat{u}}{dr} = \hat{v} = 0 \quad \text{for} \quad \begin{matrix} r = 1 \\ r = \frac{b}{a} \end{matrix} \tag{2.19}$$

Cylindrical symmetry suggests the possibility of solution in terms of Bessel functions. Taylor developed a complete set of orthogonal functions related to the Bessel functions and expanded (2.17). The resulting infinite set of homogeneous linear equations is in priciple solvable as a determinant of infinite rank, but Taylor evaluated it approximately for a number of limiting cases including the one of interest to us here-the narrow gap limit. It is assumed that the growth rate σ is real and passes through zero so that the secondary flow is also time-independent. This assumption is known as the exchange of stabilities and is justified by the nature of the disturbance as well as experiment[9]. The result of this analysis is presented in figure 2.2(a). For cylinders rotating in the same direction there is rough agreement between these results and the prediction of the Rayleigh criterion. Rigid body rotation-the diagonal dotted line- is stable. For counter-rotating cylinders there is a cylindrical surface where the velocity passes through zero. The squared circulation must decrease as that surface is approached from the inside and the flow should be unstable. There are examples where this is true of the Taylor analysis but in this case as in the case of interest to us-outer cylinder stationary;inner one rotating-there seems to be much more stability than the Rayleigh criterion allows. The conclusion is that the instability

Figure 2.2

(a) The stability boundary of Couette flow (after Taylor[8]) (b) The streamlines of the resulting secondary flow.

(a)

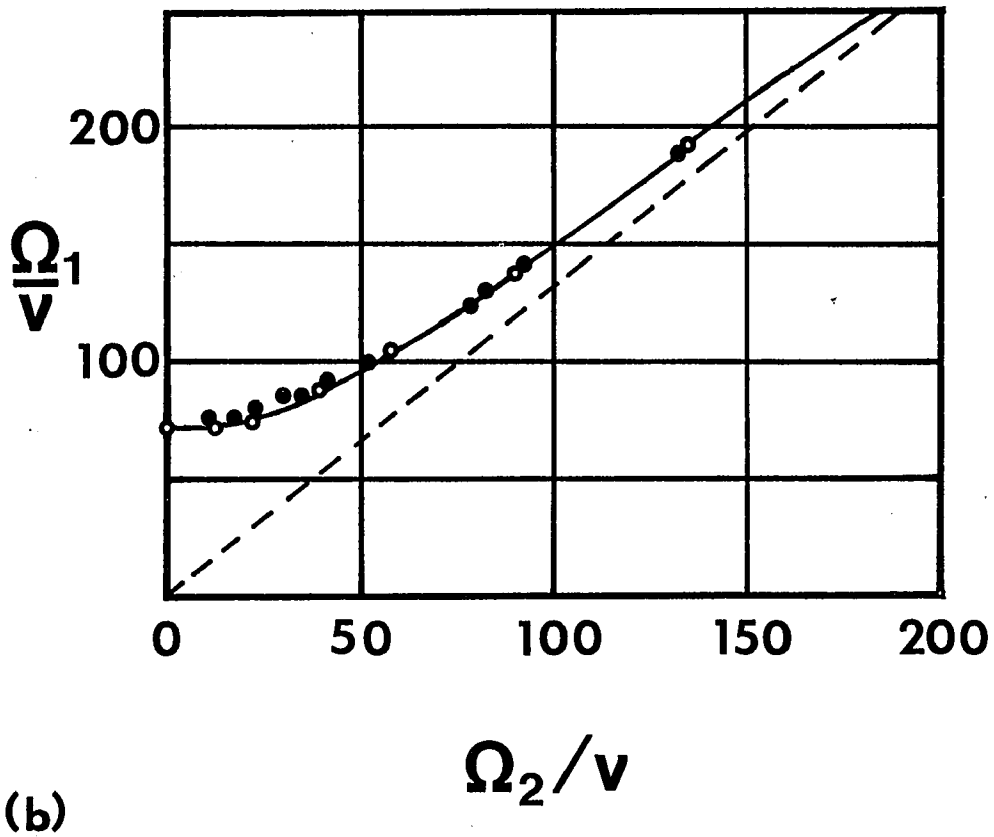

(b)

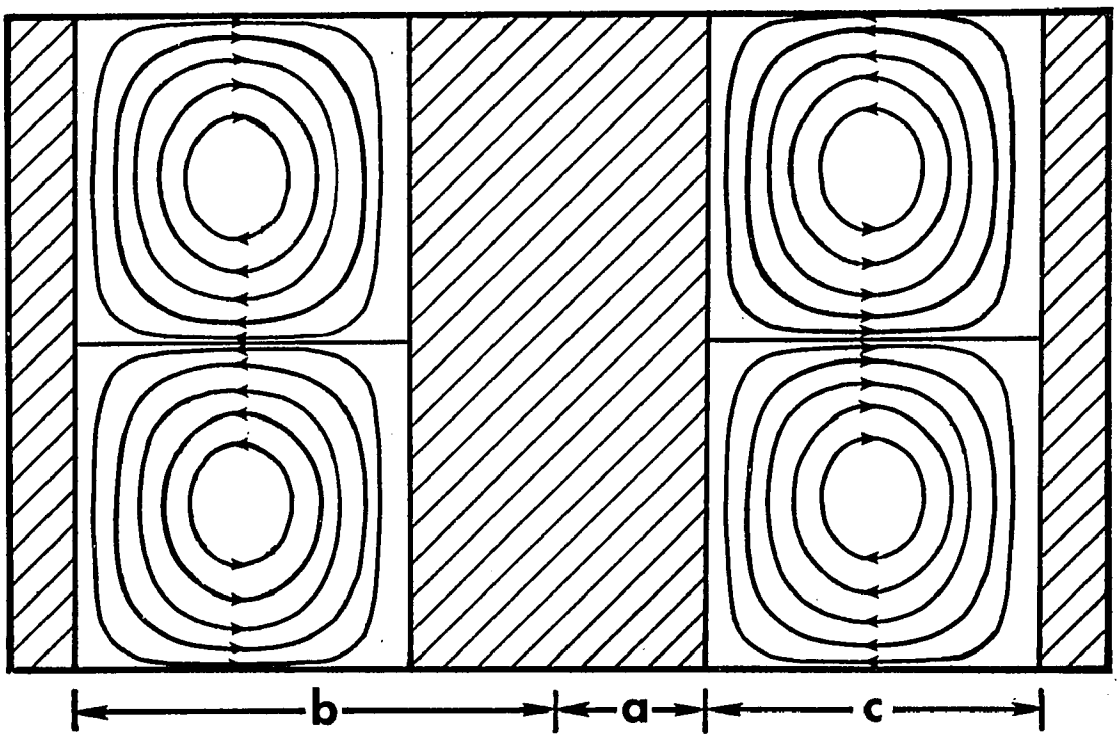

mechanism of the inviscid analysis is the mechanism of the viscous case when instability occurs, but the presence of the viscosity tends to damp it out until it finally overcomes the dissipation. A physical picture of this effect is that the viscosity adds a term to Kelvin's theorem which allows the displaced fluid element to exchange circulation with its surroundings and match up with its new environment. To our knowledge no one has attempted a refinement of Rayleigh's analysis by attempting to quantify the rate at which this equalization occurs relative to the magnitude of an unfavorable circulation gradient.

The fact that z does not appear explicitly in (2.17) indicates that the resulting secondary flow is periodic in the z-direction. Taylor was able to calculate the stream lines for selected cases and showed them to be of the form shown in figure 2.2(b) which corresponds well with the observations that originally inspired him to do the theory. The flow has lost its translational symmetry in the axial direction and has a cellular vortex structure as shown in figure 2.3(a) which is a photograph taken using a visualization method to be described in Chapter 4.

This form can be understood if we recall the inviscid analysis. We pointed out that instability is in both radial directions. Thus there is no contradiction in having a flow with outward directed flow at some values of z and inward directed at others and continuity requires it. Another

Figure 2.3

(a) R/R_c = 1.1 Time-independent Taylor vortex flow with 18 vortices. The flows at the upper and lower fluid surfaces are inward. The vertical bars are fiducials separated by 10°angles. (b) R/R_c = 6.0. (c) R/R_c = 16.0. (d) R/R_c = 23.5. Figures (b) and (c) illustrate wavy vortex flow (with 4 waves around the annulus), while in (d) the waves have disappeared. In (b), (c), and (d) there are 17 vortices, and the flow is outward at the upper surface and inward at the lower surface.

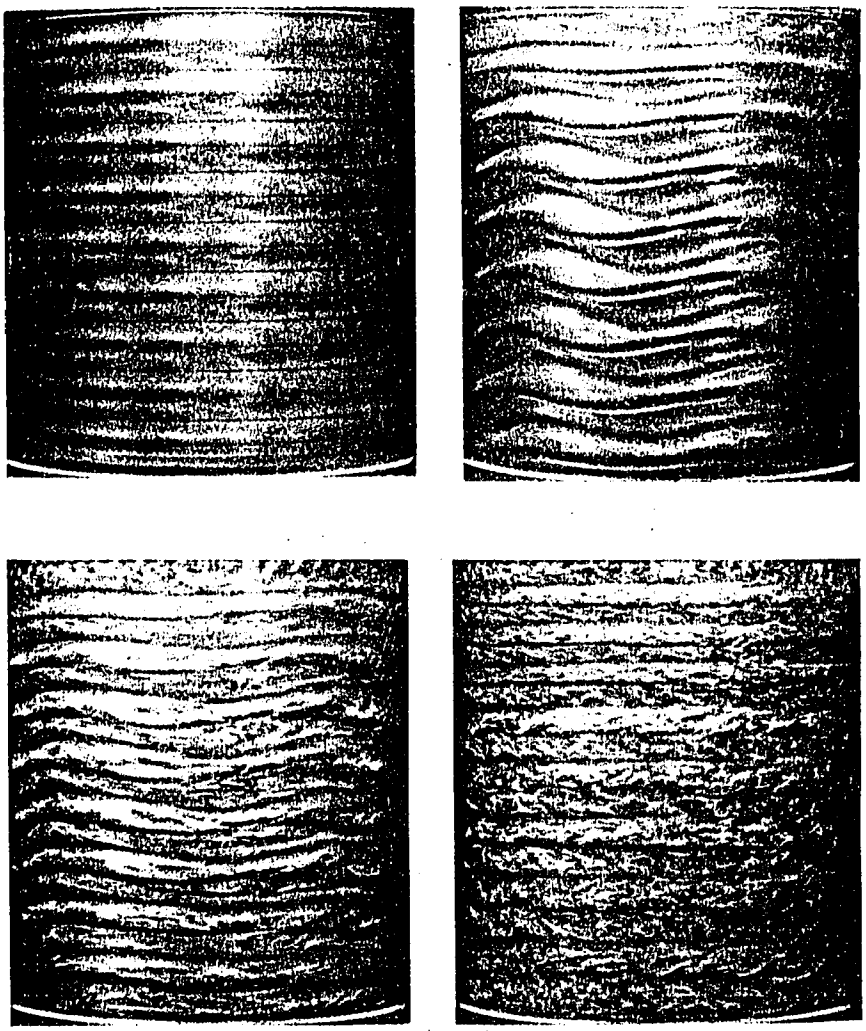

(*a*) (*b*)

(*c*) (*d*)

picture is presented by Coles[10] who considers a disturbance of a small segment of a vortex line away from the axial direction. Then as shown in Von Karman's analysis the inward displaced end will experience an inward directed force and the outer displaced end an outward directed force. The resulting torque then causes the segment to precess about the z-direction until it is parallel or anti-parallel to azimuth. Since pressure forces are radial the torque is directed in the azimuthal direction and the vortex segment ceases to precess when it is aligned in that direction.

Linear stability theory predicts unbounded exponential growth of an unstable mode. This unphysical property of the solution is understandable when we recall that the analysis is based on the assumption of small disturbances. An infinitesimal amplitude unstable disturbance obeying the linearized equations of motion will after some period of time grow to sufficient amplitude to invalidate the assumption of smallness. At that point the higher order terms ignored previously become important. Usually the these terms oppose the growth of the mode so that it saturates at a constant amplitude. Landau[11,12] presented a very simple and general argument for this type of behavior in the case of a time dependent secondary flow which predicts a dependence of the saturation amplitude on Reynolds number of the form $\sqrt{R-R_c}$. Davey[13] showed rigorously that the Landau form of the amplitude equation is valid for the case of a time-independent Taylor flow and evaluated the coefficients.

Donnelly[14] confirmed it experimentally in a semi-quantitative way. Donnelly and Schwarz[15] observed that further increases in Reynolds number lead to the appearance of harmonics of the basic axial periodicity. Snyder and Lambert[16], using hot thermistor anemometry, measured the first four Fourier coefficients of the axial waveform, the first two of which agreed well with those of Davey. Gollub and Freilich[17] introduced further expansions to Davey's work assuming smallness of the reduced Reynolds number $(R-R_c)/R_c$ and arrived at a dependence of the Fourier coefficients of the form:

$$A_p \propto [(R-R_c)/R_c]^{p/2} \qquad (2.20)$$

They measured the first four coefficients to high precision using time averaged laser Doppler velocimetry and obtained an unexpectedly good fit out to reduced Reynolds number of 2 for the case of small radius ratio (η=.61) where the Taylor vortices remain stable to $(R-R_c)/R_c \simeq 5$.

More recently J.A. Cole[18] has observed departures from the Couette solution even at modest Reynolds numbers, the effect being more pronounced in systems where the axial length is short compared to the gap width. Stable shadow vortices appear near the end while V_r is zero in the central portion of the fluid. As R is increased more cells appear at each end but the central portion remains free of radial motion until the Reynolds number is close to the appearance of secondary flow in a long apparatus. Then cells appear in

succession from the vortex regions already present at the ends. When the cells meet, the pattern then readjusts itself so that the vortices are reasonably equal in size in the z-direction. Flow in this regime is shown in Figure 2.3(b). Cole also measured the torque reaction on the outer cylinder due to rotation of the inner cylinder as a function of Reynolds number and found a change in the slope of the curve near the critical Reynolds number. His results are shown in figure 2.4. For small cell heights he found that the slope changed continuously over a fairly wide range of Reynolds number while this transition region occupied a shorter interval in Reynolds number as the cell length was increased. The center of this interval is insensitive to length. He correlated these results with the indeterminacy of visual measurements of the transition and found good agreement.

These results are qualitatively explained by the theoretical work of Benjamin[19] who showed that features of the finite cylinder problem can be obtained from the infinite cylinder problem by introducing the gap to length ratio as an imperfection parameter. For the idealized case of zero imperfection parameter the Couette solution bifurcates into two stable solutions symmetric with respect to reversal of the velocities. Finite values of the imperfection parameter cause this symmetry to be broken and the corresponding degeneracy to be lifted. The stable solution at low Reynolds number then connects smoothly with

Figure 2.4

Torque reaction on the static outer cylinder due to viscous transport of shear stress as a function of the speed of the inner cylinder for the case of c/a = 0.0940 (from Cole[18]).

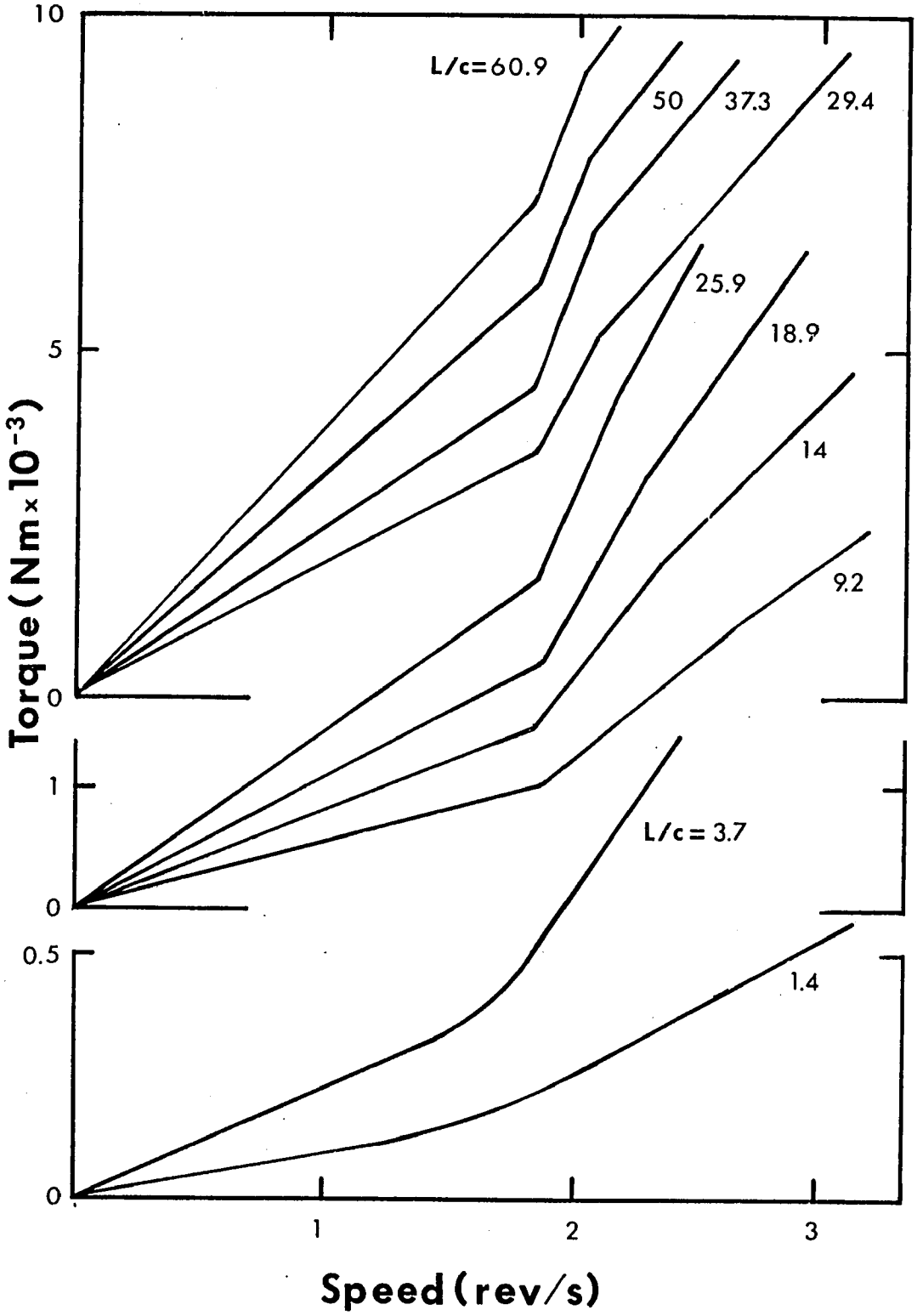
10
5
0
1
0
0.5
0
1
2
3
L/c=60.9
50
37.3
29.4
25.9
18.9
14
9.2
L/c = 3.7
1.4
Torque (Nm x 10⁻³)
Speed (rev/s)

with a curve near one of the two zero imperfection branches and the solution near the other zero imperfection branch becomes separated. This describes the softening of the Taylor transition and allows for a non-uniqueness of the flow pattern at a given Reynolds numberwhich Benjamin observed experimentally. While Benjamin's theory is the first to describe non-uniqueness, a phenomenon previously observed under different circumstances, he had the discourtesy to observe new examples to fit his theory rather than explain some of the old ones.

2.4. Wavy Vortex Flow

The time-independent flow gives way at a well defined Reynolds number to a flow which has azimuthal waves superimposed on the vortex boundaries. This flow is shown in figure 2.3(b) and was first observed by Taylor[8] and later photographed by Schultz-Grunow and Hein[20]. The motion of the waves causes the velocity to acquire a periodic time-dependence in Eulerian coordinates which we will subsequently refer to as ω_1.

The most extensive experimental study to date is that of Coles [10] who did hot wire measurements in air and flow visualizations in two liquids of this geometry. He studied the general case where both inner and outer cylinders are free to rotate over a wide range of Reynolds number and the parameter μ and for a large number of Reynolds number histories. He discovered that the number of axial and azimuthal waves is not a unique function of the Reynolds number. He also concluded that to within his experimental accuracy that the phase velocity of the azimuthal waves obeyed a universal curve independent of the wavenumber.

Davey, DiPrima,and Stuart[21] performed a monumental- and highly laborious- stability analysis of supercritical Taylor vortex flow based on a double amplitude expansion assuming infinite cylinders. This expansion is in effect an expansion of an expansion of the flow in terms of the

eigenfunctions of the linear problem and is therefore valid only for Reynolds numbers slightly above the Taylor instability. They found that for the narrow gap case there is growth of the non-axisymmetric modes at a Reynolds number close enough to the Taylor instability for the expansion to still be valid. Their results are in reasonable agreement with the previously reported experimental results of Coles[10] as far as the critical Reynolds number is concerned. Eagles[22] was able to relax the narrow gap assumption and retain the next higher term in the expansion and verified the results of Davey, Diprima, and Stuart theoretically.

One point of disagreement between the theory of Davey et. al. [21] and the experimental results of Coles was that theory predicted that the mode with one wave in the azimuth (m=1) would be the most unstable yet Coles saw the four wave mode (m=4) at the transition. Schwartz, Springett,and Donnelly[23] did an experiment with a large aspect ratio and m=1 was the first to appear. Coles apparatus, on the other hand, had a small aspect ratio.

Cole studied the transition Reynolds number as a function of aspect ratio and found a strong dependence as shown in figure 2.5.

Figure 2.5

Critical speeds for the onset of (i) Taylor and (ii) wavy vortices determined from visual observations for the case of c/a= 0.1190 which is the most nearly comparable to the current study.

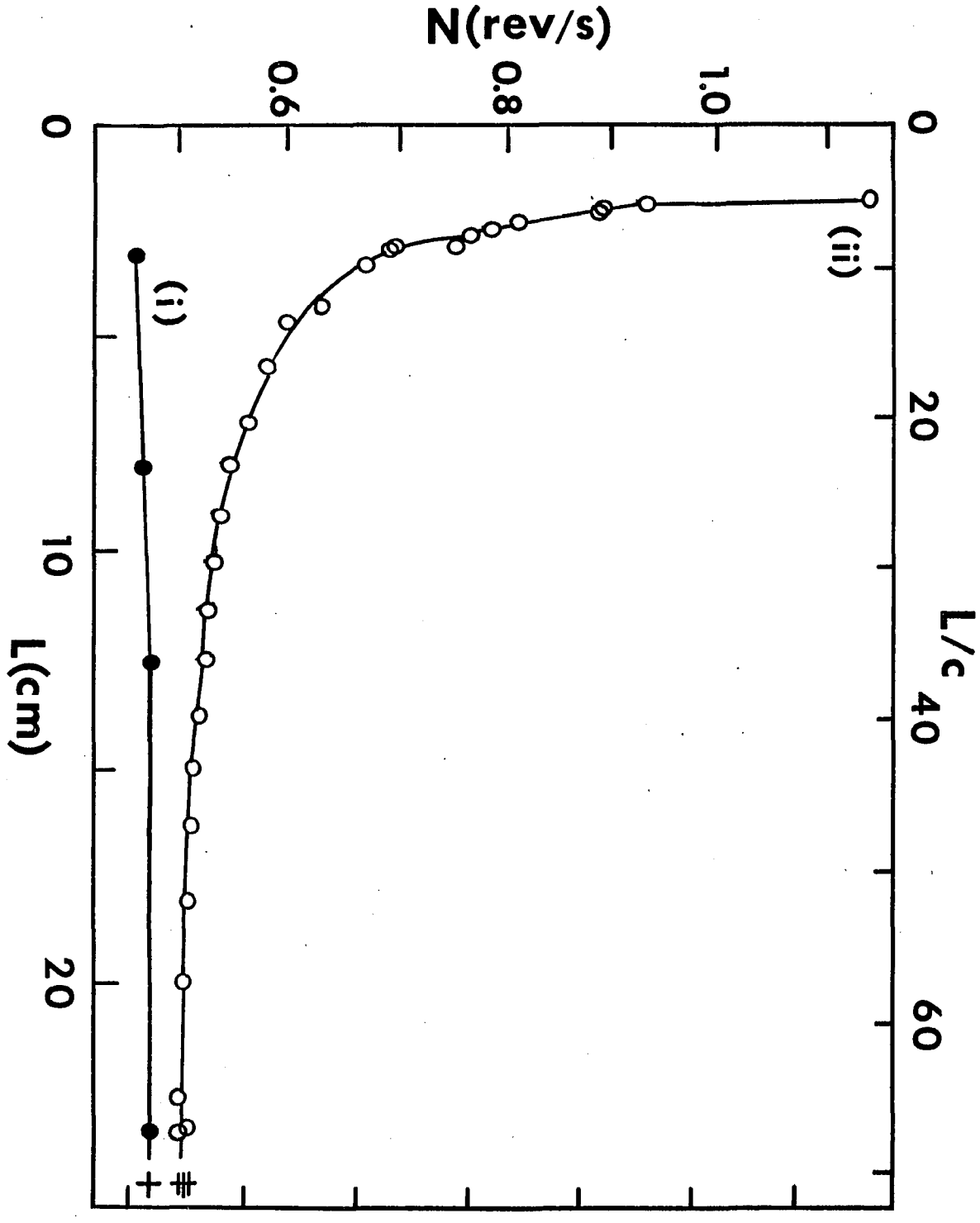
N(rev/s)
0.6
0.8
1.0
0
L(cm)
10
20
L/c
20
40
60
(i)
(ii)

2.5. Chaos

Coles observed that with further increase in Reynolds number small scale motion evolved, increasing in amplitude until the azimuthal waves eventually disappeared. This flow is shown in figure 2.3(d). He attributed the transition to turbulence to 'spectral evolution', a mechanism proposed by Landau[10,11] based on following the progression of flows that develops as the flow is adiabatically increased in speed. At very low Reynolds numbers the flow will be laminar time-independent flow. As the Reynolds number is increased it eventually reachs a value which renders the original flow unstable. A secondary flow develops and saturates in amplitude. The secondary flow is then an oscillation which grows in amplitude and eventually stabilizes at a constant value and has a definite frequency associated with it. The phase of the oscillation however, depends on the initial conditions.

With further increase in the Reynolds number it eventually reachs a value at which the secondary flow becomes unstable. A new oscillation develops and grows in amplitude eventually reaching its saturation. The flow now has two frequencies of oscillation and two phase factors dependent upon initial conditions. Further increases in Reynolds number presumably add still more frequencies and phase factors until the motion becomes "complicated and confused"[12].

This picture implies that turbulent flow is in fact quasi-periodic with the statistical character representing ignorance of the initial conditions in much the same way as it does in statistical mechanics. In figure 2.6 we show how the Landau picture appears in the form of velocity power spectra. This is a plot of how the time dependent portion of the kinetic energy is distributed in frequency space. No spectrum is displayed for the time-independent flow. Figure 2.6(a) shows the velocity power spectrum after the first instability. The single peak of non-zero frequency shows that the flow is strictly periodic. In figure 2.6(b) the prescence of two non-zero frequency peaks shows the the flow is (most likely) quasi-periodic and figure 2.6(c) shows the turbulent state where the motion is highly multiply periodic. It is to be noted that while the spectrum is highly populated all the peaks present are delta functions. In figure 2.7 we present a plot of frequencies present versus Reynolds number. We shall compare this later to similar plots. The Landau picture is impressive as an attempt to understand a highly complex non-linear phenomenon in terms of a composition of results obtained from different expansions of restricted validity.

Hopf[24] actually produced a system of non-linear equations which has the behavior described by Landau. His system:

Figure 2.6

Velocity fluctuation power spectra for the different regimes of flow in the Landau picture of the transition to turbulence. This quantity is a measure of the kinetic energy per unit frequency in the time-dependent component of the flow.

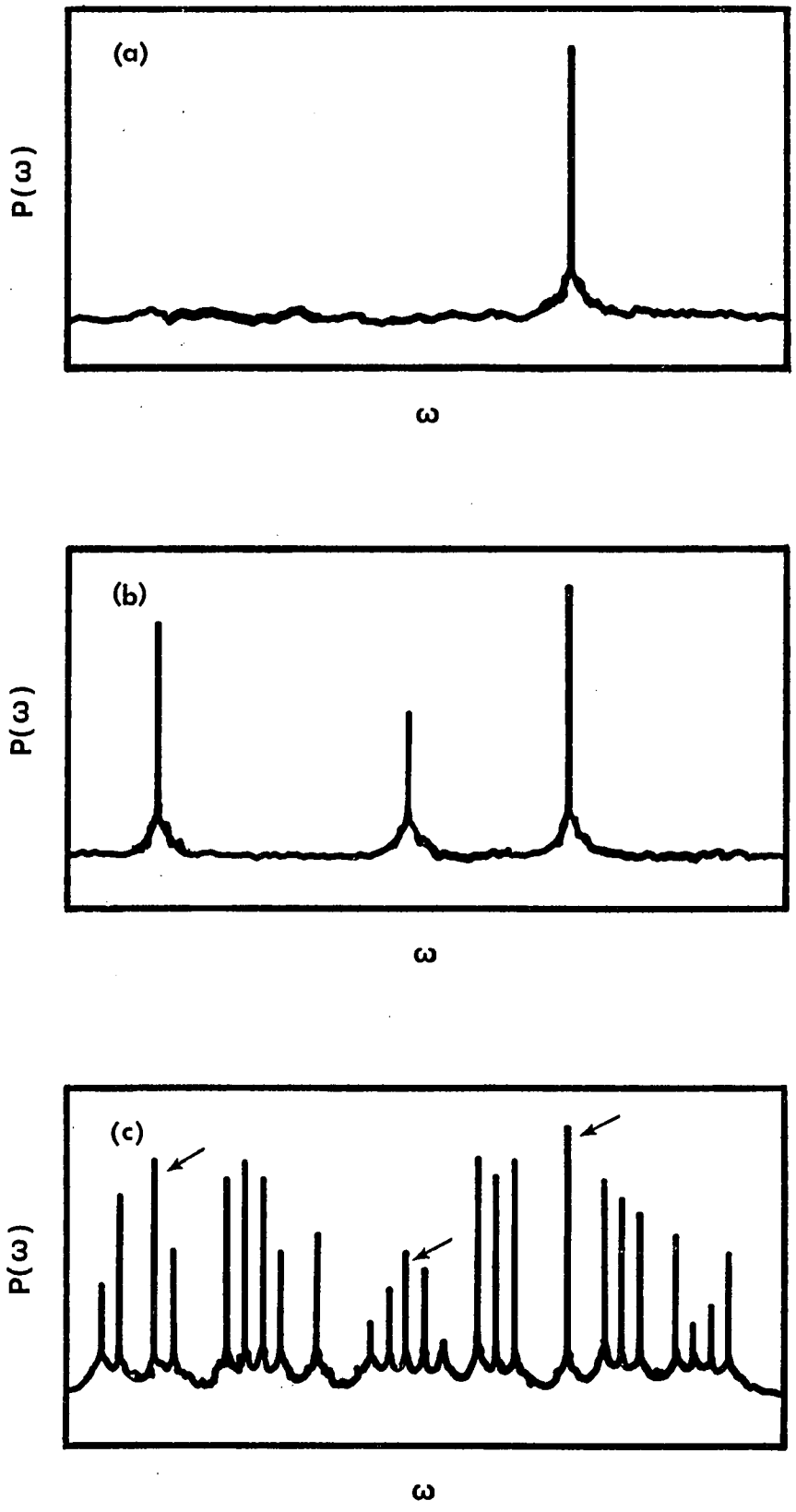
(a)
P(ω)
ω
(b)
P(ω)
ω
(c)
P(ω)
ω

Figure 2.7

A summary of the frequencies appearing in the spectra of figure 2.6 as a function of Reynolds number in the Landau picture of the transition to turbulence.

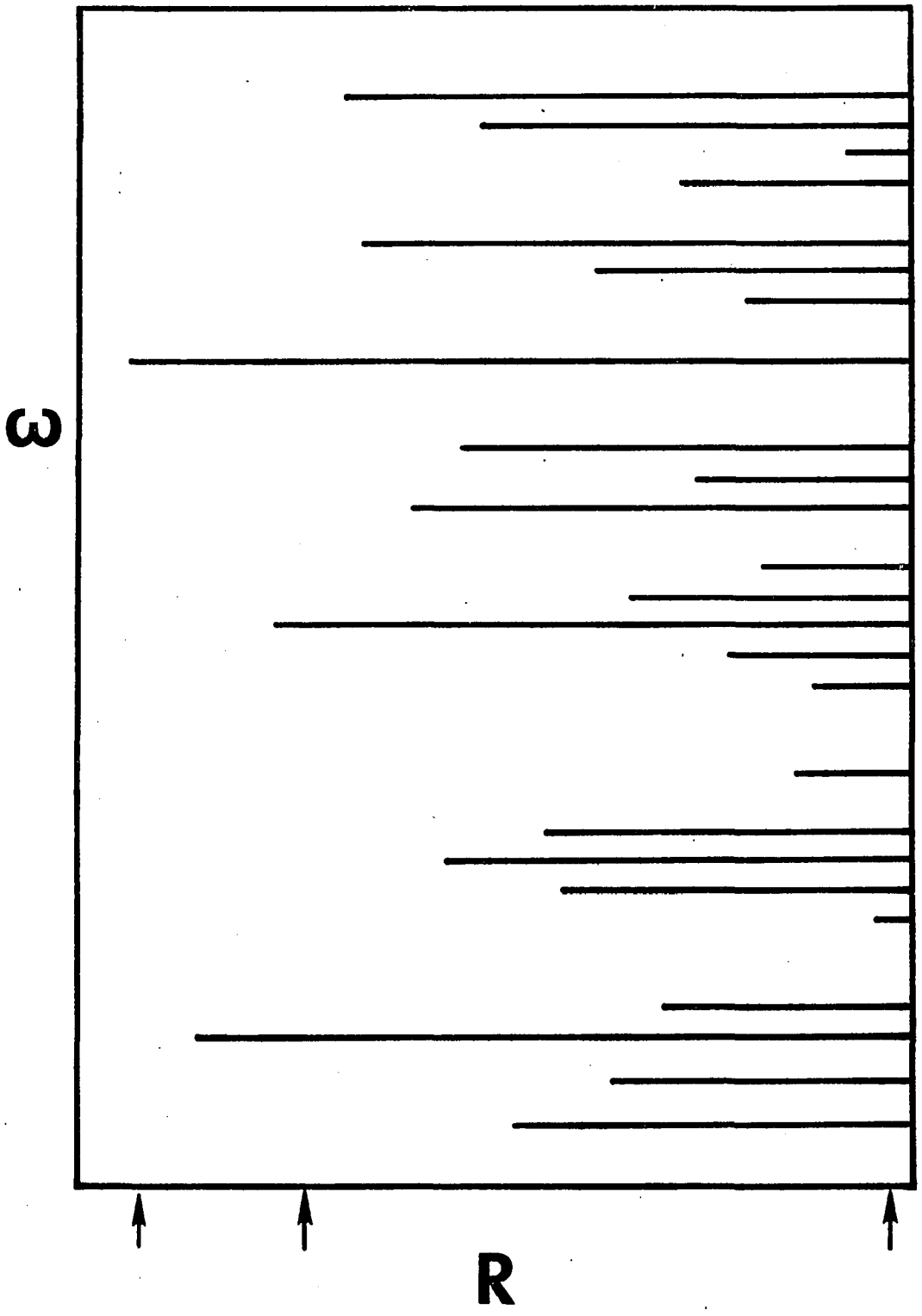
ω
R

$$\frac{\partial u}{\partial t} = -z_0 z^* - u_0 l + \mu \frac{\partial^2 u}{\partial x^2}$$
$$\frac{\partial z}{\partial t} = z_0 u^* + z_0 F^* + \mu \frac{\partial^2 z}{\partial x^2} \qquad (2.21)$$

where:

$$f \circ g = \frac{1}{2\pi} \int_0^{2\pi} f(x+y) g(y) dy$$

is the convolution integral and $F(x) = a(x) + ib(x)$ is a given function. Developing the functions u,z,a, and b in Fourier series he showed that for most initial conditions the solution tends as $t \to \infty$ toward:

$$u = \sum_{n^2\mu < a_n} (-a_n + n^2\mu) e^{inx}$$
$$z = \sum_{n^2\mu < a_n} (n^2\mu(a_n - n^2\mu))^{1/2} e^{inx} \exp\{-ib_n(t+\alpha_n)\} \qquad (2.22)$$

The summations include only terms for which $n^2\mu < a_n^2$ .This has two consequences. First, there are only a finite number of terms in any solution. Second, the number of frequencies increases as μ decreases (or as R increases). This development strengthened belief in the Landau picture. Hopf, however, cautioned that the applicability of his results to hydrodynamics was unclear because the non-linearity of the later case is very different in character from the type he chose to study. Later we will apply the benefit of hindsight to his speculation.

Gollub and Swinney[25] did real time laser Doppler velocimetry in a relatively short apparatus of the same ratio

of radii as that used by Coles in an effort to find additional time-dependent instabilities above the wavy vortex instability and below Reynolds numbers where the flow is clearly turbulent. Surprisingly, they

found only three such instabilities. They also observed a fourth instability component of the velocity power spectrum that was not resolvable with their resolution into discrete frequencies. The resulting suspicion of the Landau conjecture and the absence of any detailed analytic theory of these higher Reynolds number instabilities led to a search for theories having some qualitative correspondance to observation.

One class of such theories was inspired by the work of Lorenz[26] who studied a system of equations due to Saltzman[27]. Saltzman was interested in the progression of flows in a fluid between parallel planes where the lower plane is at a higher temperature than the upper. The Rayleigh-Benard instability is well known but behavior as the temperature difference of the plates is increased was not theoretically understood. Saltzman developed the equation of motion for the system- the Bousinessq equations- in Fourier series and integrated a finite number of terms numerically. He discovered that in certain cases all but three of the dependent variables went to zero and the nonvanishing variables underwent irregular, apparently nonperiodic fluctuations. Lorenz discovered that the same

solutions could be obtained if only the three lowest order terms are retained. The result is the system:

$$\begin{aligned} \dot{X} &= -\sigma X + \sigma Y \\ \dot{Y} &= -XZ + rX - Y \\ \dot{Z} &= XY - bZ \end{aligned} \qquad (2.23)$$

where X, Y, and Z are the amplitudes of the three modes retained. He studied this system numerically and found that at high values of the parmeter reminiscent of the Rayleigh number (temperature difference), solutions varyied aperiodically in time. Thus he showed that chaotic solutions can be contained in a system of equations having only a few degrees of freedom.

Another class of theories was originated by Smale[28] as a part of his development of the subject of differential dynamical systems. This is an outgrowth of global analyis which attempts to ascertain properties of solutions of differential equations in the large by applying topological arguments to the mappings on differentiable manifolds that correspond to the equations. Dynamical systems is the restriction to the study of equations that represent physical systems. Smale produced the first example of what is now known as a strange attractor. This is a region of phase space which is attracting but in which no orbit is stable. The orbits are typically hyberbolic, that is, the are attracting in some directions and repelling in others.

Ruelle and Takens[29] proposed a model for turbulence in a similar vein. They showed that for "most" nonlinear differential equations a strange attractor appears "near" a triply periodic solution so that chaos is observed after two time-dependent instabilities. Ruelle[30] has also shown that the Lorenz system displays a strange attractor but with a single hysteretic time-dependent instability before the onset of chaos.

A very recent experimental study by Walden[31] shows that the the critical Reynolds number for the disappearance of the wavy vortices is dependent upon the aspect ratio of the apparatus. For aspect ratios somewhat larger than used in the current study he found that after the initial disappearance of the waves they would reappear at a higher Reynolds number and disappear again at a still higher Reynolds number. A summary plot of his results is shown in figure 2.8. He refers to this phenomenon by the provacative name of "reemergent order".

Figure 2.8

Summary plot of the Reynolds numbers at which the vortex waves appear and disappear as a function of aspect ratio (from Walden[31]).

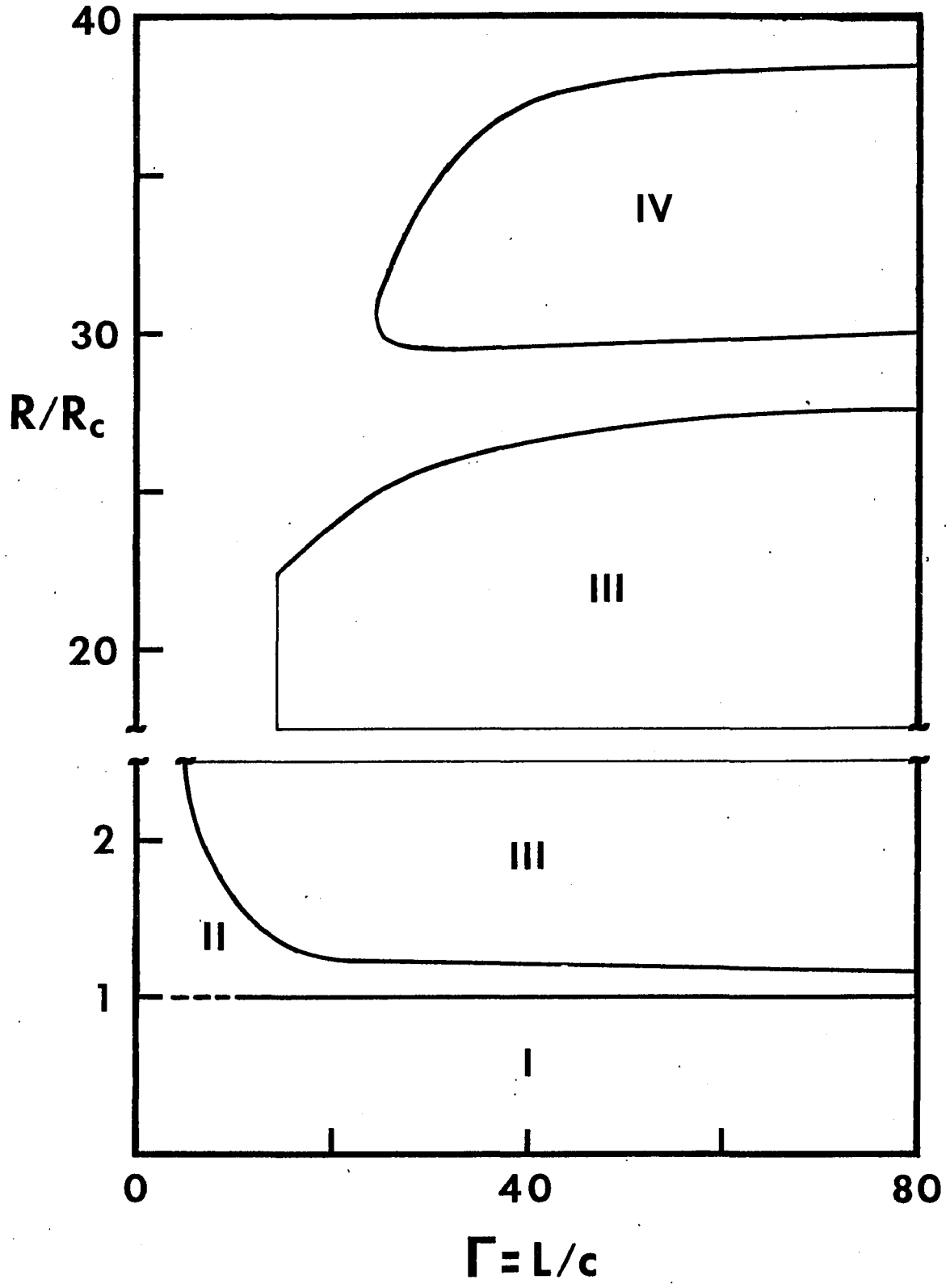
40
30
20
R/Rc
IV
III
2
1
III
II
I
0
40
80
Γ = L/c

References for Chapter II

1. Richardson, S. 1973 On the no-slip boundary condition. J. Fluid Mech. 59, 707.

2. Couette, M. 1890 Etudes sur le frottement des liquides. Ann. Chim. Phys.(6),21, 433.

3. Mallock, A. 1896 Experiments on fluid viscosity. Phil. Trans. A 187, 41-56.

4. Rayleigh, Lord 1920 On the dynamics of revolving fluids. Scientific Papers 6, 447-453.

5. Karman, Th. von 1934 Some aspects of the turbulence problem. Proc. 4th Int. Congr. Appl. Mech.,Cambridge, England. Reviewed in [9] pp.49-50.

6. Synge, J.L. 1933 The stability of heterogeneous liquids. Trans. Roy. Soc. of Canada, 27, 1-18. Reviewed in [7] pp. 280-281.

7. Chandrasekhar, S. 1961 Hydrodynamic and Hydromagnetic Stability. Oxford: The Clarendon Press.

8. Taylor, G.I. 1923 Stability of a Viscous Liquid between Two Rotating Cylinders. Phil. Trans. Roy. Soc. London A, 223, 289.

9. Lin, C. C. 1966 The Theory of Hydrodynamic Stability. Cambridge: Cambridge University Press

10. Coles D. 1965 Transition in circular Couette flow. J. Fluid Mech. 21, 385-425.

11. Landau, L. 1944 On the problem of turbulence. C.R. (Dokl.) Acad. Sci. URSS 44, 311-315.

12. Landau, L. and Lifshitz, E.M. 1959 Fluid Mechanics, Reading Mass.: Academic Press, pp. 103-107.

13. Davey, A. 1962 The growth fo Taylor vortices between rotating cylinders. J. Fluid Mech. 14, 336-368.

14. Donnelly, R.J. 1963 Experimental confirmation of the Landau law in Couette flow. Phys. Rev. Lett. 10, 282-284.

15. Donnelly R.J. and Schwarz, K.W. 1965 Experiments on the stability of viscous flow between rotating cylinders. VI. Finite-amplitude experiments. Proc.Roy. Soc. A 283,531-556.

16. Snyder, H.A. and Lambert, R.B. 1966 Harmonic generation in Taylor vortices between rotating cylinders. J Fluid Mech. 26, 545-562.

17. Gollub, J.P. and Freilich, M.H. 1976 Optical heterodyne test of perturbation expansions for the Taylor instability. Phys. Fluids 19, 618-625.

18. Cole, J.A. 1976 Taylor-vortex instability and annulus-length effects. J. Fluid Mech. 75, 1-15.

19. Benjamin, T.B. 1978 Bifurcation phenomena in steady flows of a viscous fluid. I. Theory. II. Experiments, Proc. Roy. Soc. A. 359, 1-26 and 27-43.

20. Schultz-Grunow, F. and Hein, H. 1956 Beitrag zur Couettestromung. Z. f. Flugwiss. 4,28-30

21. Davey, A., DiPrima, R.C., and Stuart, J.T. 1968 On the instability of Taylor vortices. J. Fluid Mech. 31, 17-52.

22. Eagles, P.M. 1971 On the stability of Taylor vortices by fifth-order amplitude expansions. J. Fluid Mech. 49, 529-550.

23. Schwarz, K.W., Springett, B.E. and Donnelly, R.J. 1964 Modes of instability in spiral flow between rotating cylinders. J. Fluid Mech. 20,281-289.

24. Hopf, E. 1948 A mathematical example displaying features of turbulence. Comm. Pure Appl. Math., 1,303.

25. Gollub, J.P. and Swinney, H.L. 1975 Onset of turbulence in a rotating fluid. Phys. Rev. Lett. 35, 927-930.

26. Lorenz, E.N. 1963 Deterministic nonperiodic flow. J. Atm. Sci. 20, 130-141.

27. Saltzman, B. 1962 Finite amplitude free convection as an initial value problem. J. Atmos. Sc. 19, 329-341.

28. Smale, S. 1967 Differential Dynamical Systems. Bull. Am. Math. Soc. 73, 747.

29. Ruelle. D. and Takens, F. 1971 On the nature of turbulence. Commun. Math. Phys. 20,167-192

30. Ruelle, D. 1976 The Lorenz attractor and the problem of turbulence. Quantum Dynamics:Models and Mathematics,Streit, L.,ed., New York: Springer-Verlag.

31. Walden, R.W. 1978 Transition to turbulence in Couette flow between concentric cylinders. Ph.D. thesis University of Oregon.

3. THE LASER DOPPLER TECHNIQUE

3.1. General

Since its conception by Yeh and Cummins[1] Laser Doppler velocimetry (LDV) has emerged as the single most powerful method for precision fluid velocity measurements. LDV is actually a specialized form of the more general subject of light beating spectroscopy. As the name implies this technique utilizes the wave interference properties of light to detect small changes in frequency as the light is scattered by a sample medium. This technique can be used to study a broad class of fluctuation and diffusion phenomena[2]. LDV is the restriction of light beating spectroscopy to the case of scattering from small seed particles imbedded in a fluid flow. In this case the scattering is essentially elastic in the particles' own frame of reference and the resulting Doppler shift frequency in the lab frame can be understood very simply in terms of Galilean transformations between the frames. The particles are massive enough to average out molecular structure, yet small enough to be regarded as mass points on the fluid dynamic length scales.

Much of the power of the Laser Doppler Velocimetry (LDV) technique derives from the wide disparity between the length and time scales characteristic of the laser radiation and those characteristic of fluid flows. A laser beam can be focused to a spot size reasonably close to the diffraction limit. Typical values for the parameters used in LDV setups

limit. Typical values for the parameters used in LDV setups are shown in table I. The probe volume dimension is appropriate to the hydrodynamic description of a many particle system, where the length scale is chosen to be large compared to molecular dimensions and small compared to the size of the sample. Also shown in table I are the approximate number of molecules in the probe volume and the ratio of the longest probe volume dimension to the scale of the apparatus. It is the large size of these numbers which justifies the previous assertion.

Table I

Length Scales

Molecular dimension	10^{-8} cm
Probe volume dimension	10^{-3} cm
Apparatus dimension	10^{-1} cm
Number of molecules in probe volume	10^{+15}
Ratio Apparatus/Probe dimension	10^{+2}

Time

Optical Period	10^{-15} sec
Doppler Period	10^{-5} sec
Fluid wave period	10^{-1} sec
Ratio Fluid/Doppler	10^{+4}

In the time domain similar considerations apply. Again refering to Table I we see that for typical parameters, the time scales are widely separated. We shall return to this point in the discussion of detection schemes where we will

with which a given detection scheme can measure a time-dependent flow.

Additional advantages of LDV over other velocity measuring techniques are its non-perturbative character and the fact that the LDV response to velocity is intrinsically linear in the velocity. The former is particularly important in the case of a closed system where any perturbation of the flow due to the probe will be retained in the flow and reappear at the probe. The later is in contrast to a probe like the hot-wire where the response is non-linear in the velocity and requires correction of the raw data with a calibration curve.

While it should in principle be possible to measure fluid velocities by scattering light directly from the fluid itself, in practice this is not done since the scattering is in general too weak and the resulting light scattering spectrum is so broad -in the megahertz range- that it obscures the Doppler shift. Thus it is convenient experimentally to seed the fluid with particles which are small enough to follow the flow faithfully but large enough to scatter light strongly and without introducing undue spread to the light scattering spectrum. The character of seed particles is not always a matter of choice. In complicated flows of engineering interest it is frequently necessary to use particles already present in the flow. In the present study of a controlled laboratory flow it is possible to

study of a controlled laboratory flow it is possible to select the type and concentration of seed particles. In this case spherical particles are the natural choice since they will not lead to large changes in the signal amplitude as they change orientation with respect to the probe. Further it is easier to optimize the scattering from spherical particles since their properties have been studied more extensively than more general shapes.

3.2. Particle Motion

The use of seed particles requires an analysis of how faithfully they follow the flow to be studied. We shall first consider the equation of motion appropriate to a single particle immersed in a fluid and later discuss briefly collective particle effects. The independent particle problem in fullest generality has not been solved. We will use an approximate form and later justify the neglect of effects which for our case are small. The most general form which has been successfully dealt with is:

$$\frac{\pi d^3}{6}\rho\frac{dV}{dt} = \quad \text{Particle inertia}$$

$$-3\pi\mu d(V-U) + \quad \text{Stokes drag}$$

$$\frac{\pi d^3}{6}\rho_0\frac{dU}{dt} \quad \text{Pressure drag} \qquad (3.1)$$

$$-\frac{1}{2}\frac{\pi d^3}{6}\rho_0\frac{d(V-U)}{dt} \quad \text{Inviscid drag}$$

$$-\frac{3}{2}d^2\sqrt{\pi\mu\rho_0}\int_0^t\frac{d(V-U)}{d\xi}\frac{d\xi}{\sqrt{t-\xi}} \quad \text{Basset term}$$

where V and U are the particle and fluid velocities respectively, ρ_0 is the density of the fluid, ρ is the density of the particle, d is the particle diameter, and μ is the shear viscosity.

The first term is simply the force required to accelerate the particle. The second term is the viscous drag

as calculated by Stokes[3]. This form is only valid for low Reynolds numbers relative to the sphere, but this condition is met in a surprisingly large number of cases. Its correctness in a given application can be approached in two ways. First it can be taken as an ansatz and justified a posteriori or it can simply be noted that the higher order corrections to the Stokes formula are negative so that the estimate of particle fidelity neglecting them will be conservative and therefore acceptable. The third term in (3.1) is an expression of the pressure gradient that results across a particle as a result of an acceleration of the imbedding fluid. The fourth term is the drag of an inviscid fluid on a sphere and represents the force necessary to accelerate the mass added by replacing the fluid in a particle volume with a particle. The first, third, and fourth terms are sometimes lumped together into the 'virtual mass' term.

A great deal of work has been done on the solution to (3.1). For our purposes we shall refer to a review article by Hjelmfelt and Mockros[4]. The solution for the particle motion is developed in terms of the Fourier integral and its relationship to the Fourier integral of the fluid motion:

$$U = \int_0^\infty \{\zeta \cos(\omega t) + \lambda \sin(\omega t)\} d\omega$$

$$V = \int_0^\infty [\eta\{\zeta \cos(\omega t+\beta) + \lambda \sin(\omega t+\beta)\}] d\omega \qquad (3.2)$$

where ζ and λ are arbitrary constants and:

$$\eta = \sqrt{(1+f_1)^2+f_2^2} \qquad (3.3)$$

represents the relative amplitude of the particle motion and:

$$\beta = \arctan\left(\frac{f_2}{1+f_1}\right) \qquad (3.4)$$

represents the relative phase angle. The functions f_1 and f_2 are given by:

$$f_1 = \frac{\omega(\omega+c\sqrt{\pi\omega/2})(b-1)}{(a+c\sqrt{\pi\omega/2})^2+(\omega+c\sqrt{\pi\omega/2})^2}$$
$$f_2 = \frac{(a+c\sqrt{\pi\omega/2})(b-1)}{(a+c\sqrt{\pi\omega/2})^2+(\omega+c\sqrt{\pi\omega/2})^2} \qquad (3.5)$$

where:

$$a = \frac{18\nu}{\{(\rho/\rho_0)+\frac{1}{2}\}d^2}$$
$$b = \frac{3}{2\{(\rho/\rho_0)+\frac{1}{2}\}} \qquad (3.6)$$
$$c = \frac{9}{\{(\rho/\rho_0)+\frac{1}{2}\}d}\sqrt{\frac{\nu}{\pi}}$$

We would like to evaluate the response of particles immersed in water characterized by:

$$\rho_0 = .996 \text{ gm/cm}^3 \qquad \rho = 1.05 \text{ gm/cm}^3$$
$$\nu = .845 \text{ cs} \qquad d = 4.81 \times 10^{-5} \text{ cm} \qquad (3.7)$$

immersed in water. Substituting the above values into (3.5) and assuming an angular frequency of $2\pi \times 10^5$ we have:

$$a = 4.25 \times 10^7 \text{ sec}^{-1} \qquad f_1 = 5.71 \times 10^{-5}$$
$$b = .968 \qquad f_2 = 1.65 \times 10^{-7} \qquad (3.8)$$
$$c = 6.26 \times 10 \text{ sec}^{1/2} \qquad \eta \simeq 1 + f_1$$

Substituting these values into (3.3) we see that such

particles deviate from the fluid motion by less than 1 part in 10^{+4} at a frequency of 100kHz which is orders of magnitude beyond frequencies of interest.

Effects not included in (3.1) which are sometimes important are:

$$V = \frac{d^2 g}{18\mu_0}(\rho - \rho_0) \qquad \text{Gravity}$$

$$F = \frac{1}{4}\pi\rho_0 (V-U) d^3 \Omega \qquad \text{Magnus Effect}$$

$$F = 20(U-V)d^2\left(\mu_0\rho_0\frac{dU}{dy}\right)^{1/2} \qquad \text{Shear Flow Lift} \qquad (3.9)$$

$$\frac{V_r}{V_t} = \frac{\omega d^2(\rho - \rho_0)}{18\mu} \qquad \text{Centrifugal response}$$

where g is the gravitational constant, F is force on the particle, Ω is the angular velocity of rotation of the particle, V_r and V_t are the radial and tangential components of the particle velocity, and ω is the angular velocity of rotation of the mean flow. Gravity can be discounted due to the small difference between the density of the particle and that of the surrounding fluid and more importantly due to small particle size. The centrifugal response can also be neglected due to small particle size. The Magnus effect, which results from rotation of the particle, and shear flow lift, which results from the presence of a velocity gradient across the particle, both require the existence of a relative velocity from another

source and therefore can also be neglected.

There is one final effect we would like to mention which is not contained in the fluid model of the imbedding medium. The size of particle we have been considering is massive enough to average out most of the random impulses from individual molecular collisions. However, the random occurrence of many similarly directed impulses simultaneously is observable. This is the well known Brownian motion which is described as a random walk process. If we designate $\Delta R(t)$ the length of the random jump at time t, the the Einstein-Stokes[5] results are:

$$\begin{aligned} \langle \Delta R \rangle &= 0 \\ \langle (\Delta R(t))^2 \rangle &= 6Dt \\ D &= \frac{kT}{6\pi\eta a} \end{aligned} \tag{3.10}$$

where k is the Boltzman constant, T the absolute temperature, η the shear viscosity, and we assume ergodicity so that the brackets may indicate either time or ensemble averaging. We see that the particle will on the average follow the flow but fluctuate about it. For the many particle case of interest to us, the effect these fluctuations have on the estimation of the fluid velocity can most easily be evaluated directly from the light scattering spectrum and will be discussed later.

Until now we have considered only a single particle.

Even in the case where there is only one particle at a time in the probe volume it is still true that there are many particles immersed in the fluid. One must then ask whether the single particle equations of motion are adequate to describe their behaviour. At a concentration typical of our experiments of $n = 10^{-2}\,\mu^3$the mean free path for hard sphere collisions is about 800 diameters so that interaction can be neglected. The next possibility to consider is the hydrodynamic interaction, that is the force one particle exerts on another by perturbing the fluid flow in its vicinity. As we have shown above particles of interest to us are fixed in the fluid to an excellent approximation so that they do not perturb the flow and do not interact hydrodynamically. Finally there is the possibility of surface charge resulting in an electrostatic interaction. In de-ionized double quartz distilled water this effect can sometimes be a problem, but in ordinary singly distilled water, ions in solution screen these charges over a very short range. Therefore one should not expect to see collective particle effects.

3.3. Light Scattering

The interaction of light with matter allows determination of many aspects of material structure. For our purposes, however, we would like to restrict ourselves to elastically scattered light. We consider a configuration as shown in figure 3.1(a). The illuminating radiation represented by:

$$\vec{E}_0(t) = \vec{E}_0 e^{i(\vec{k}_i \cdot \vec{x} - \omega_0 t)} \tag{3.11}$$

impinges on a spherical particle of different index of refraction from the imbedding medium. A number of theories describe the scattered field in different cases, but they have in common that the far field is representable as:

$$\vec{E}_s(t) = \frac{\overleftrightarrow{S}(\theta,\phi)\cdot\vec{E}_0}{4\pi|\vec{R}-\vec{r}|} e^{i\cdot\vec{k}\{(\vec{R}-\vec{r})-\omega_0 t\}} \tag{3.12}$$

The scattering theories then differ in the evaluation of $\overleftrightarrow{S}(\theta,\phi)$. Normally one would expect a 3x3 matrix relating two vectors, but since the vectors represent the independent directions of polarization, they are two-dimensional and the scattering matrix is 2x2. For spherical particles the matrix is diagonal and its elements are independent of the angle ϕ. Theories come in three basic varieties which in historical order are Rayleigh scattering, Rayleigh-Gans-Debye theory and Mie theory. Rayleigh theory is true for particles of arbitrary shape provided that they are small enough. Then it is possible to assume that the electric and magnetic fields are of uniform magnitude and phase across the dimensions of the particle. The scattering may then be

Figure 3.1

(a) The kinematics of a light scattering event. The momentum transfer vector $\vec{q} = \vec{k}_i - \vec{k}_s$ and θ is the scattering angle. (b) The reference beam LDV geometry. The reference beam r goes directly in to the photomultiplier while light scattered through an angle from the illuminating beam i mixes with it. (c) A cross-section of the measuring control volume in the plane defined by the two intersecting beams. The parallel lines represent the 1/e intensity points of the individual beams and the boundary of the hatched region is the locus of 1/e intensity points of the combined beams.

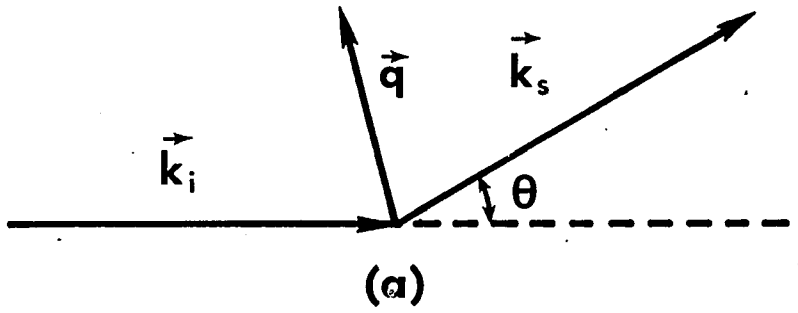

(a)

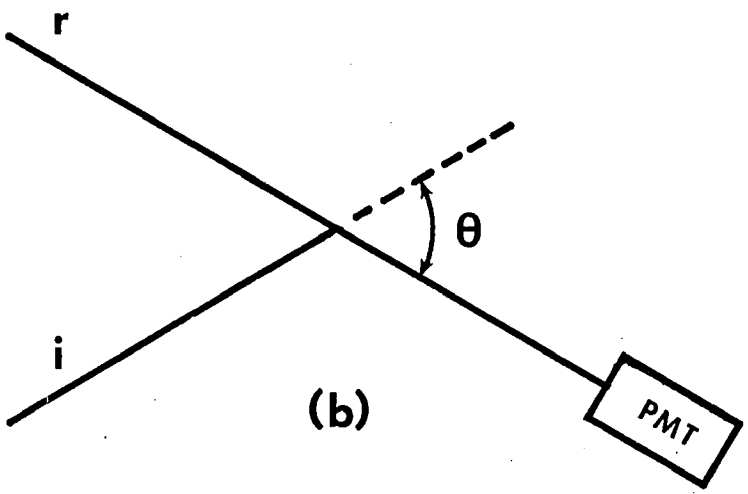

(b)

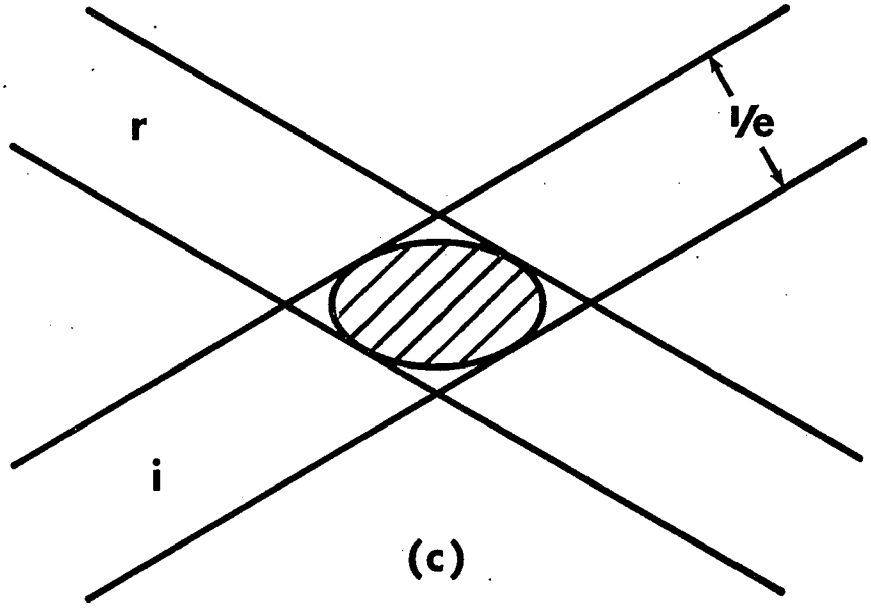

(c)

attributed to an induced oscillating dipole moment at the center of the particle and its magnitude can be calculated from the electrostatics of macroscopic media with time appearing only parametrically. The result of this calculation gives:

$$\overleftrightarrow{S}(\theta,\phi) = ik^3\alpha\begin{pmatrix}\cos\theta & 0\\ 0 & 1\end{pmatrix} \tag{3.13}$$

where m is the relative index of refraction between the particle and the surrounding medium, k is the magnitude of the incident propagation vector and a is the particle radius and:

$$\alpha = \frac{(m^2-1)d^3}{(m^2+2)} \tag{3.14}$$

is calculated from the Lorenz theory of the polarization of a dielectric sphere. The most important feature for us at the moment is the third power dependence of the scattered amplitude on the radius of the particle, which leads to a sixth power radius dependence in the intensity. Also the scattering intensity is symmetric between the forward and backward directions. This suggests that one should use the largest possible particle provided it can still follow the flow faithfully. In fact we will see that the desirable size of particles actually fall outside the assumptions of the Rayleigh theory.

A theory which generalizes the Rayleigh theory to particles of larger size is the Rayleigh-Gans-Debye theory.

However, this generalization is made at the expense of the additional requirement that the relative index of refraction of the scatterer be close to unity. This allows one to assume that the illuminating and scattered waves are not appreciably shifted in relative phase as they traverse the dimensions of the particle. The result of this theory is:

$$\overleftrightarrow{S}(\theta,\phi) = ik^3d^3(m-1)\left(\frac{2\pi}{u^3}\right)J_{3/2}(u)\begin{bmatrix}\cos(\theta) & 0\\ 0 & 1\end{bmatrix} \qquad (3.15)$$

where:

$$u = 2kd\sin(\theta/2) \qquad (3.16)$$

and the criterion for its applicability is:

$$\frac{4\pi}{\lambda}d|m-1| << 1 \qquad (3.17)$$

This type of scattering has a more complicated dependence on radius than Rayleigh scattering and also increasingly favors forward scatter as particle size increases. The optimal size within the applicability of the theory may depend sensitively on the scattering geometry, but because we would like to get as much scattering as we can, we would like to examine particles which are both larger than this theory permits and have large relative index of refraction.

The general theory of the scattering of light from small spherical particles of arbitrary size and material properties was first worked out in detail by Mie[6]. This theory is a full vector solution to the Maxwell equations. The case of interest for us here is the case of non-conducting non-absorbing dielectric spheres. The solution does not have a simple closed form, but can be developed in

an expansion of Sonine polynomials. Results for a large number of cases have been tabulated[7]. The intensity of the scattering is appreciably less than that predicted by a simple extrapolation of Rayleigh theory asymptotically approaching a radius squared dependence for very large particles. Thus we are still interested in using large particles where we can. Depolarized scattering can occur even for particles that are made of a material with an isotropic polarizability. The scattered intensity for particle sizes on the order of the wavelength of the illuminating radiation and larger is mostly in the forward direction which indicates that forward scattering is to be preferred when it is practical. However, even in backscatter, the increase in total scattered intensity with increasing radius is faster than the forward biasing[7]. Except for a few special cases, light scattering considerations encourage the use of the largest particles possible.

3.4. The Doppler Shift

Once we can evaluate the scattering of light by a static particle we can easily generalize to the case of a moving particle. The illuminating beam is defined in laboratory coordinates. A coordinate transformation is applied to describe it in the particles frame of reference. The frequency in this frame will not be the same as the lab frame. The scattering theories described in the previous section can then be applied. A second coordinate transformation must then be made to desribe the scattered light relative to the detector which is tied to laboratory coordinates. For low particle velocities Galilean transformations prove adequate and the result for the Doppler shift is:

$$\omega_D = \vec{U}\cdot\vec{q} = \frac{4\pi n}{\lambda_0} \sin(\theta/2)\, U_q \qquad (3.18)$$

where $\vec{U}$ is the vector velocity of the particle, $\vec{q}=\vec{k}_i - \vec{k}_s$ is the momentum transfer vector, n is the index of refraction of the fluid, λ_0 is the free space wavelength of the light, is the scattering angle, and U_q is the component of the velocity in the direction of the momentum transfer of the scattering.

3.5. Photodetection

To obtain the information about particle motion that the scattered optical field contains, it must be detected. The most sensitive and versatile methods available currently make use of the photoelectric effect in which a photon is absorbed by an atom and an electron emitted. A practical photodetector must of course be made of many photosensitive atoms and must also provide a means of restoring the emitted electrons so that the atoms can respond to later photon arrivals. The output of such a system will then be proportional to the number of photons arriving per unit time, which is just the intensity of the incident optical field. The important observation is that a photodetector responds to the field intensity rather than the field amplitude. The discreteness of the electronic charge results in an inescapable random noise component of the resulting signal called shot noise. There can be additional noise contributions due to the statistical properties of the incident photon field.

Modern amplitude stabilized lasers are to a good approximation constant intensity sources which have a intensity probability distribution:

$$p(I)dI = \delta(I-\langle I\rangle) \tag{3.19}$$

and the associated photoelectron distribution:

$$p(n,T) = (n!)^{-1}\langle n\rangle^{n} e^{-\langle n\rangle} \tag{3.20}$$

the probability of detecting n photons in a time T, is a Poisson distribution[8]. The variance of this distribution is:

$$\langle(\Delta n)^2\rangle = \langle n\rangle \tag{3.21}$$

which results in the shot noise component of the photocurrent. A Gaussian random field on the other hand has an intensity probability distribution:

$$p(I)dI = \langle I\rangle^{-1} e^{-I/\langle I\rangle} \tag{3.22}$$

which leads to a photoelectron distribution:

$$p(n,T) = \frac{1}{[(1+\langle n\rangle)(1+1/\langle n\rangle)^n]} \tag{3.23}$$

which has variance:

$$\langle(\Delta n)^2\rangle = \langle n\rangle+\langle n\rangle^2 \tag{3.24}$$

This leads to an 'excess' noise term in the photocurrent. Later we will explain why we need to consider both types of field, but for now let us simply state that tne field to be detected is essentially an amplitude stabilized laser field with a small Gaussian componenet superposed.

3.6. The Reference Beam Geometry

Figure 3.1(b) shows a typical reference beam optical arrangement. Two beams, usually derived from the same laser, are focused and brought to an intersection at their beam waists. This is not the arrangement used in the current study but its properties are more readily apparent and the correspondance to the setup actually used can be made. Since a relatively small amount of the illuminating light is scattered, the illuminating beam is usually much more intense than the reference beam. A scatterer at the beam intersection can scatter light out of the illuminating beam into the direction of the through transmitted reference beam. The resultant electric field amplitude on the photodetector is:

$$\vec{E}_T(t) = \vec{E}_s(t)+\vec{E}_r(t) \qquad (3.25)$$

where the subscripts T, r, and s indicate the total, reference, and scattered electric field amplitudes respectively. Since the photodetector responds to the field intensity, the photocurrent is proportional to:

$$I \alpha |\vec{E}_s(t)+\vec{E}_r(t)|^2 = |\vec{E}_s|^2+|\vec{E}_r|^2+\vec{E}_s^*\cdot\vec{E}_r e^{i\omega_D t} +\vec{E}_r^*\cdot\vec{E}_s e^{-i\omega_D t} \qquad (3.26)$$

where use has been made of (3.11) and (3.18). The first two terms represent a time-independent component of the photocurrent while the last two are the mixing terms. The ratio of time-dependent to time-independent current is called the heterodyne efficiency. The difference frequency of the optical fields which appears in the photocurrent due to the mixing terms is usually convenient to handle by

ordinary RF techniques and is precisely the Doppler shift frequency. Not explicitly shown above is the shot noise. Due to its presence one would like to operate at the highest light levels possible. Unfortunately photodetectors have rather stringent limits on the intensity they can accept. Thus the heterodyne efficiency becomes important as a measure of the signal to shot noise ratio.

From (3.26) we can see that the heterodyne efficiency is a maximum if the scattered light and the reference beam are of equal intensity. In practice one tries to adjust the relative intensities of the illuminating and reference beams so that this is true. Since the scattered intensity is proportional to the illuminating intensity, we can determine the effective volume from which interferering fields originate by considering the intersection of two focused equal intensity laser beams each represented by:

$$I(x,y,z) = I_0 e^{-(x^2+y^2)/r_0^2+ikz} \qquad (3.27)$$

in a coordinate system with the z-axis in the beam direction. The time-dependence has been suppressed. The resulting intensity distribution is a multivariate Gaussian with surfaces of equal intensity forming ellipsiods. A cross-section of the 1/e intensity ellipsoid is shown in figure 3.1(c) where the 1/e intensity widths of the intersecting beams is shown. The principal axes of this ellipsoid are given by[9]:

$$\Delta x = 2r_0/\cos(\theta)$$
$$\Delta y = 2r_0 \qquad (3.28)$$
$$\Delta z = 2r_0/\sin(\theta)$$

where θ is the scattering angle and r_0 is the diffraction limited waist radius of a single focused beam. The later can be calculated from:

$$r_0 = \frac{\lambda}{\pi}\frac{f}{2r_\mu} \qquad (3.29)$$

where λ_0 is the wavelength of the light, f is the focal length of the lens, and r_μ is the radius of the unfocused beam at the 1/e intensity point. The volume defined by (3.28) is called the measuring control volume.

Another property which affects the heterodyne efficiency is the coherence of the scattered light. We will develop this topic in two parts. First, we consider the influence of Brownian motion on the spectrum of light scattered from a single particle. This is of interest in its own right for its influence on signal detection to be discussed later. We then consider the many particle case where it affects the solid angle over which light can be collected without degrading the heterodyne efficiency.

As previously mentioned the light scattered by a particle is at the incident frequency in its own frame of reference and shifts observed in the lab frame are due to particle motion. For a stationary particle, where the frames of reference are the same, one might expect all the

scattering to be at the incident frequency. However, a particle undergoing Brownian motion will introduce a frequency shift during a random step and in general a different shift during the next step. If we assume the illuminating light is perfectly monochromatic so that it is a single infinite wave train, the scattered light is not, since each step of the random walk is of finite duration. The resulting scattered wave is then a superposition of finite wave trains with a distribution of characteristic frequencies. Both aspects lead to a broadening of the spectrum, the relative importance of each depending on the velocities of the steps and their durations. However, the combined effect can be evaluated in a variety of ways[10] and leads to a spectrum for the scattered light:

$$I(\omega) \propto \frac{q^2D}{(\omega-\omega_0)^2+(q^2D)^2} \qquad (3.30)$$

where q^2 is the squared magnitude of the momentum transfer vector, ω_0 the frequency of the illuminating light, and D the diffusion coefficient from (3.10). When viewed in the time domain it is easy to see that the Gaussian time distribution of steps in the random walk leads to a Gaussian time-dependence of the optical fields and that we have just described the "excess" noise discussed in (3.24).

In the many particle case, the particle motions are assumed to be uncorrelated and the spectrum is the same as for a single particle, but a new feature arises due to the spatial distribution of particles. Each particle is a

source of a scattered wave with random shifts in the phase. Thus the collection of particles in the measuring control volume acts like an extended incoherent quasi-monochromatic source. The classical theory of coherence is adequate to describe this situation and more specifically, in the common case where the distance to the detector is large compared to the source dimensions, the van Cittert-Zernike theorem applies. Calculations have shown that a reasonable estimate of the area over which the wave from such a source is in reasonable phase agreement is[11]:

$$A_{coh} = \frac{\lambda^2}{\Omega} \tag{3.31}$$

where λ is the wavelength of the light and Ω is the solid angle that the source subtends at the detector. Theoretical and experimental work has shown that the heterodyne efficiency is optimized if no more than one coherence area falls on the detector[11].

If the collection optics are arranged to collect light over one coherence solid angle (the solid angle for which the coherence area just fills the detector), it is required that the flow be heavily seeded in order to obtain enough light to get good signal quality and to reduce the phase noise due to the random entry and exit of particles from the probe volume. This choice of seeding then determines the means of electronic signal processing. The resulting signal in the reference beam case can be viewed as a frequency modulated signal with center frequency at the Doppler shift appropriate to the mean velocity. The signal processing

required is similar to the process of FM detection.

3.7. Signal Processing

In the steady flow case the velocity information can be extracted from the photodetector output by a spectrum analyzer. The velocity then is determined by locating the peak of the photocurrent power spectrum and calculating the velocity through (3.18). The photocurrent spectrum in this case consists of a single peak whose width is determined by three effects. Brownian motion contributes a width q^2D as shown in (3.10) and (3.30). In (3.28) we showed that the apparatus is sensitive to a finite volume. If the velocity varies appreciably across the measuring control volume, particles at different points within the volume will induce different Doppler shifts on the scattered light. Since the total scattered field is the sum of these contributions, the resulting light beating spectrum will have a width proportional to the magnitude of the velocity gradient across the volume. This effect is referred to as velocity gradient broadening. The third effect contributing to spectral width is called transit time broadening and results from the fact that the phase of the light scattere by a single particle is coherent only over the time Δt that it takes to cross the measuring control volume. The result is a contribution to the spectral width $\propto 1/\Delta t$. The presence of these effects complicates the problem of finding the peak of the spectrum as described later.

The case of fully developed turbulence can also be

studied in this way if the flow is statistically stationary. The photocurrent power spectrum is in this case, however, the convolution of the light scattering spectrum and the velocity fluctuation spectrum of the turbulence. The large difference in the intrinsic widths of these two spectra makes it fairly easy to extract the turbulence spectrum from the total. However, this method intrinsically restricts one to measuring the second order velocity moments. All higher moments have been discarded in the spectrum analyzer.

In recent years electronic signal processsing for LDV applications has developed to the point where it is possible to record the velocity directly in real time. There are both continuous time and discrete time methods available but we describe the discrete time method since it is easier to understand. We define a time step Δt such that it is large compared to the typical Doppler period and small compared to the period of the fluid modes. The photocurrent is spectrally analyzed over the time interval Δt . The peak of the spectrum is found, the corresponding velocity for the time step determined, and the result recorded. We proceed to the next time step by again spectrally analyzing for the time interval Δt , finding the spectral peak, calculating the velocity and recording the result as the velocity for the that time step. The velocity record (actually a histogram) is then the collection of photocurrent spectral peak estimates taken from successive spectra. This process is displayed graphically in figure 3.2.

Figure 3.2

(a) The photocurrent spectrum of the ideal Doppler signal due to beating of the Doppler shifted light with the reference beam. The spectrum is evaluated over a time interval including many Doppler cycles, but short compared to the fluid dynamic time scales. The peak frequency is at the Doppler shift frequency. (b) Contourograph of a sequence of photocurrent spectra for successive time intervals for the case of periodic time-dependent flow. The dashed curve connecting the peaks shows the time-dependence of the velocity. (c) The time series resulting from recording the peak frequency for each interval of (b). It is basically the intersection of the contourograph with the plane of contact parallel to the ω-t-plane. (d) The velocity fluctuation power spectrum from the squared modulus of the complex Fourier transform of (c).

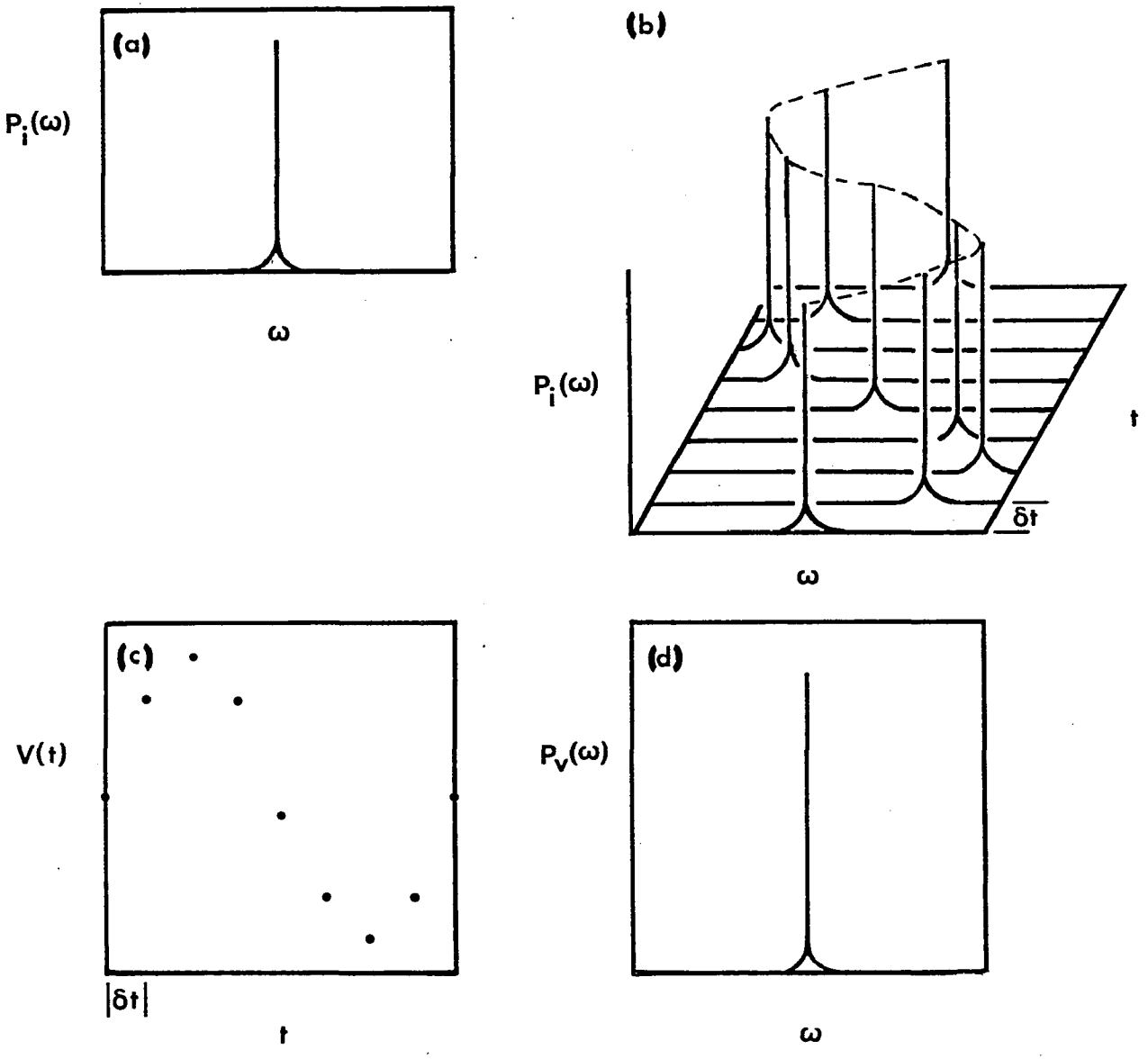
(a)
$P_i(\omega)$
ω
(b)
$P_i(\omega)$
t
δt
ω
(c)
V(t)
$|\delta t|$
t
(d)
$P_V(\omega)$
ω

A very simple scheme is frequency counting. Here the signal is conditioned so that it is a square wave with amplitude compatible with standard digital logic levels. A sampling interval is chosen long compared with the Doppler period but short compared with the fluid dynamic time scales. The Doppler cycles are then counted for the duration of the sample interval and the resulting count stored in a location of computer memory. Subsequent time intervals are similarly counted and the results stored in sequential locations of memory. This technique has rather poor signal to noise characteristics, but it has the advantages that it is inexpensive and easy to interface to a computer.

Since the Doppler shift frequency appears in the photocurrent spectrum along with noise, any measurement of it will be an estimator drawn from an ensemble of estimators centered on the true spectrum. As a result the frequency of the peak extracted from such an estimate will itself be an estimate. Figure 3.3(a) shows the photocurrent spectrum for a single time step as in figure 3.2(a), but in this case including noise. The peak occurs at ω_0 (observed) rather than ω as before. Since this displacement is due to random noise we should expect it to be different for each time step and the resulting observed velocity record fluctuates about the true record as shown in figure 3.3(b). If the true record is a sine wave, the observed velocity power spectrum will have a single sharp peak with a white noise background as in figure 3.3(c). Note that the magnitude of this effect

Figure 3.3

(a) A single time interval photocurrent spectrum for a real Doppler signal with a peak frequency differing from the Doppler frequency. The dashed curve is the ideal spectrum from figure 3.2(a). The dotted curve is the assumed noise spectrum and the solid curve is the sum. (b) The resulting time series comparable to figure 3.2(c) where the solid curve shows the time variation of the true signal and the individual points show random fluctuations due to the effect shown in (a). (c) The resulting velocity fluctuation spectrum comparable to figure 3.2(d) which now has a background noise component.

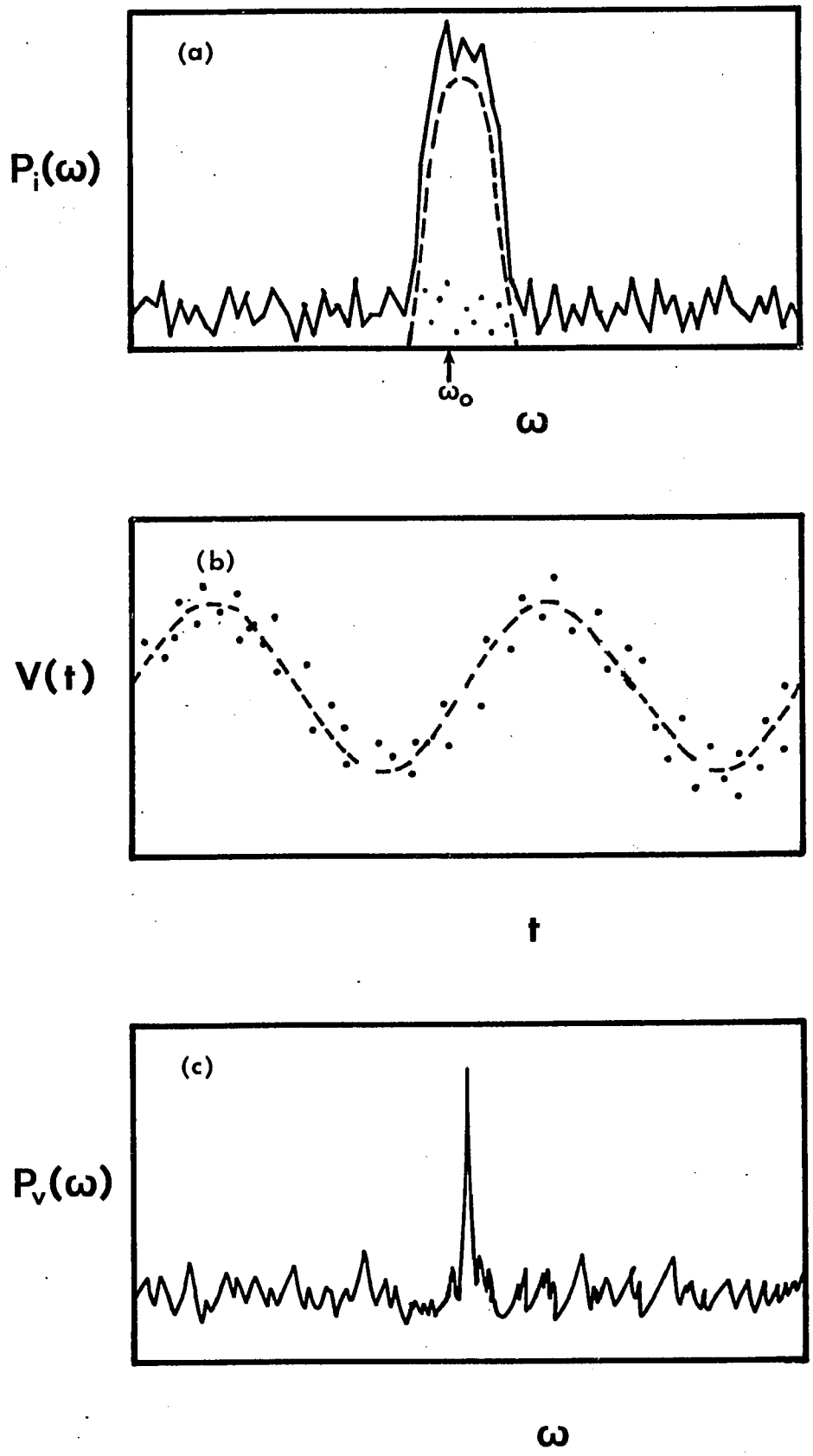
(a)
$P_i(\omega)$
ω_o
ω
(b)
V(t)
t
(c)
$P_v(\omega)$
ω

depends on the width of the signal peak and the background noise level. Usually the signal width is determined by Brownian motion, transit time broadening, or velocity gradient broadening and the noise is shot noise which is white. As a result, it is usually desirable to bandpass filter the photocurrent since reducing the bandwidth will proportionately reduce the noise power admitted into the signal processor. The signal power will remain unaffected as long as the bandpass is wider than the signal peak.

Another effect removed by the high pass portion of the filtering is due to the fact that the scattered and reference beams do not have equal intensities everywhere in the measuring control volume. As we saw in connection with defining that volume, unequal intensities lead to incomplete interference. For a static particle this would lead to a d.c. bias to the photocurrent. For a moving particle this leads to a low frequency contribution to the photocurrent. This is the reference beam analog of an effect called pedestal in the fringe geometry.

3.8. Data reduction

The most common form of data reduction is to construct the velocity power spectral density. In the case of fully developed turbulence, the wavevector spectrum is the obvious choice for comparison with theory, since most theories attempt to derive this quantity from a truncated moment equation hierarchy. In the case of the onset of chaos the frequency spectrum is the convenient language to express the Landau conjecture and other newer theories as mentioned in Chapter 2. The output of a real-time LDV processor can be reduced to this form by either analog or digital methods, the convenient choice often determined by the technology of the processor. Some aspects of method are common to both approaches; some are unique to one.

A power spectral density can be constructed from a data record by three methods, filtering, construction of the autocorrelation function and subsequent Fourier analysis, and the squared modulus of the Fourier transform. In the filter technique, one detects the power transmitted through a narrow bandpass filter. The spectrum is then constructed by recording the output as the filter is scanned across the frequency range of interest. The disadvantage is that most of the signal power is rejected while only that which is in the bandpass contributes to the accumulation of the output. The alternative is to use a bank of parallel filter-detector channels, but this drastically increases the cost. The

second method, called the Blackman-Tukey method, is a direct application of the Wiener-Khinchin theorem and was popular before the advent of the Fast Fourier transform (FFT). For reasons of statistical consistency (to be described later) one usually calculates significantly less autocorrelation coefficients than samples in the record. If M is the number of coefficients computed and N the record length, the complexity of the calculation is of order MN, which is an improvement over the N complexity of a direct discrete Fourier transform (DFT) of the record. However, the time compexity of the FFT of order N ln N, is less than that of the autocorrelation calculation when N is large which makes the third method the best choice.

If we assume that a component of velocity is a continuous real-valued function on the infinite time domain, we see that distortions must enter when we try to represent it in any other form. All methods have a spectral resolution limited by the finite duration of a measurement and all measurements are, due to the presence of noise, statistical estimates of the true values. This leads to the subjects of leakage suppression and statistical consistency, respectively. Reducing the continuous time domain to discrete equal length time intervals causes the apparent frequency of some excitations to be very different from the real frequency, while reducing the continuous range of values of the function to the discrete values representable in digital form leads to the presence of a noise background

in the spectra. These are the subjects of aliasing and quantizing noise, respectively. These four effects will be discussed in order.

A pure monochromatic wave requires an infinite wavetrain, whereas a collection of frequencies can comprise a finite duration wavetrain. A finite duration measurement cannot discriminate between the two cases. Therefore, there is an intrinsic loss of spectral resolution. The observed record can be viewed as the convolution of a finite length data window with the real infinite duration signal. From the convolution theorem of Fourier analysis we have that the resulting spectral estimate is the product of the true spectrum with the spectrum of the data window. If no special processing is performed, the window has the form of a top-hat function in the time domain:

$$u(t) = \begin{matrix} 1 & |t| < T/2 \\ 0 & |t| > T/2 \end{matrix} \qquad (3.32)$$

which has the transform:

$$u(\omega) = \frac{2\sin(\omega T/2)}{\omega} \qquad (3.33)$$

and resulting spectrum:

$$P(\omega) = \frac{4\sin^2(\omega T/2)}{\omega^2} \qquad (3.34)$$

This later form is undesireable due to the presence of side lobes separated from the main lobe by null points. It is possible to reduce the total amount of spectral energy in the side lobes at the expense of a slight broadening of the main lobe by weighting the input data with a function that is tapered near the ends of the record. Simple functions such as the cosine can be used effectively, but experience

has shown that the GEO[12] window to be a higher performance algorithm in digital applications. Windowing has an added benefit when the FFT is used in the construction of the PSD. Unlike the DFT which can provide Fourier coefficients on a mesh arbitrarily close together in frequency space, The FFT gives a fixed sampling of coefficients. If the nodes of transform of the top-hat fall exactly on the points provided by the FFT the resulting estimate of the spectral width will be too small. This effect is alleviated if a window is applied before the transform is taken for then the transform of the window does not have nodes close to the main lobe.

Due to the presence of noise, each measurement of the velocity that appears in the record is a statistical estimate drawn from a distribution centered on the true value. Therefore, the record can be viewed as a collection of random variables which is mapped by the construction of the PSD into another collection of random variables. For a statistically consistent estimate one must have the variance of the estimates decrease as the number of samples increases. The normal use of the method described previously yields a spectrum which has an incresing density of points in the frequency domain as the record length is increased, so that the number of samples contributing to a given estimate of a spectral point does not increase. Therefore, there is no improvement in the variance of an individual point. One method of reducing the variance is to collect additional records and average them together. The variance

of a specific velocity estimate input to the PSD is reduced and the resulting output inherits that property. Equivalently, several separately constructed spectra may be averaged. A method that uses only one record is averaging neighboring channels of the PSD estimate. This reduces the variance at the expense of the frequency resolution.

Aliasing results from the division of the continuous time domain into equal length discrete slices. Exactly one value of the dependent variable is recorded for each time slice. Signal variations which occur on a time scale that is small compared to the size of the time step cannot be represented without distortion. Fortunately this distortion has a predictable form. If a sine wave has a frequency $f=1/2\Delta t$ where Δt is the interval between samples, the resulting record consists of values equal in magnitude and alternating in sign. It is possible to deduce the original signal from this representation, but for higher frequencies the samples will vary in magnitude and some sign reversals will be missed, causing the record to appear to be that of a lower frequency. The frequency $1/2\Delta t$ assumes a central role in the evaluation of aliases and is called the Nyquist folding frequency. The relationship of the observed frequency f_o to the real frequency f when $nf_c < f < (n+1)f_c$ is[12]:

$$\begin{aligned} f_o &= f - nf_c \quad \text{for } n \text{ even} \\ f_o &= (n+1)f_c \quad \text{for } n \text{ odd} \end{aligned} \tag{3.35}$$

This effect is usually handled by being sure that the signal

is band limited below the folding frequency by a filtering technique.

Digitizing noise results from the reduction of a continuous variable to a representation by a fixed length binary number which can take on only a finite number of values. In general, the value of the continuous variable will fall between values of the binary representation, so that the digitizing hardware must assign a value which is in error by as much as $\pm 1/2$ the value of the least significant bit. Unless some special relationship exists between the continuous variable and the representable binary numbers, the errors will tend to be evenly distributed over the interval equal in length to the value of the least significant bit and will have an essentially white spectrum. The amplitude of the noise is determined by the ratio of the least significant bit value to the largest value representable and is therefore a function only of the word length. For 10 bit quantization, the digitizing noise is 83 db. down from the signal level[12]. In our work this is negligible.

References for Chapter III

1. Yeh, Y. and Cummins, H. Z. 1964 Localized Fluid Flow Measurements with a He-Ne Laser Spectrometer. Appl. Phys. Lett. 4,176-178.

2. Berne, B.J. and Pecora, R. 1976 Dynamic Light Scattering. New York: Wiley.

3. Lamb, H. 1945 Hydrodynamics. New York: Dover pp. 602-603.

4. Hjelmfelt, A.R. and Mockros, L.F. 1966 Motion of discrete particles in a turbulent fluid. Appl. Sci. Res. 16, 149 -161.

5. Ref. 2 p. 82.

6. Mie, G. 1908 Ann. Physik, 25, 377 reviewed in Ref. 7 pp.114-130.

7. Van de Hulst, H. C. 1957 Light Scattering by Small Particles. New York: Wiley.

8. Wolf, E. and Mehta, C. L. 1964 Determination of the Statistical Properties of Light from Photoelectric Measurements. Phys. Rev.Lett. 13, 705-707.

9. Durrani, T. S. and Greated C. A. 1977 Laser Systems in Flow Measurement. New York: Plenum.

10. Corsignani, B., DiPorto, P., and Bertolotti, M. 1975 Statistical Properties of Scattered Light. New York: Academic Press.

11. Cummins, H. Z. and Swinney, H. L. 1970 Light Beating Spectroscopy. Appeared in Wolf, E., ed.,Progress in Optics, Vol. VIII. Amsterdam: North-Holland.

12. Otnes, R.K. and Enochsen, L. 1972 Digital Time Series Analysis. New York: Wiley.

4. Experimental Techniques

The flow is parametrized by the Reynolds number, the ratio of radii, and the ratio of the gap to the cell length. Thus the measurement and control of these variables is the major portion of the fluid mechanic technique required. Values for the scale lengths are:

Inner Cylinder Radius	r_i	2.224 cm.
Outer Cylinder Radius	r_o	2.536 cm.
Gap	c	0.312 cm.
Fluid Height	L	6.25 cm.
Aspect Ratio	L/c	20.0
Ratio of Radii	η	0.877

A uniform and stable rate of rotation of the inner cylinder is obtained by the use of a synchronous motor driven by the output of a precision oscillator. The period of rotation is determined by an electronic timer and is stable to within $\pm$0.3% in ten cycles. The temperature of the water must be controlled since the viscosity varies by approximately 2%/^{0}C. This is achieved by a proportional controller with a thermistor sense input which drives a heating element inside a box enclosing the entire sample portion of the apparatus. A fan provides circulation to make the temperature uniform in the region of the flow cell. This gives a constant temperature to within $\pm$.05 C which implies a constant viscosity to within 1 part in 1000. For laser Doppler measurements the flow is seeded with 0.361μm or 0.488um spheres at a concentration of 0.03% or 0.06% by volume which changes the viscosity by only 0.05% or 0.1% respectively[1]. Most measurements were made with the viscosity fixed at its value at 27.5 ^{0}C, but some

measurements were also made at 30 ^{0}C and 60 ^{0}C. No significant difference was observed in the velocity power spectra obtained at the same Reynolds number with different rotation frequencies and viscosities. No significant differences are observed when the particle size or concentration are changed, confirming that Brownian motion and collective particle effects can be neglected.

The number of axial waves is determined by comparison of the position of velocity maxima with values determined from visualization which are accurate to $\pm$8% of a cell. Subsequent measurements in a given run are made after a quasistatic change in speed with periodic remeasurement of the state. The number of azimuthal waves can also be determined by correlating visualization data with the laser Doppler measurements. In visualization the number of azimuthal waves can be determined directly from stop action photographs. At the same time measurements of the reflected intensity of a Helium-Neon laser provide the frequency of the fluid motion due to the waves passing a fixed point in the sample. This makes it possible to identify the number of waves in the laser Doppler measurements. In the next section we hope to show that the geometric parameters-Reynolds number, gap to cell length ratio, and ratio of radii-together with axial wavenumber, and azimuthal wavenumber give a unique characterization of the flow.

The optical front end of the laser Doppler velocimetry

system is shown schematically in figure 4.1(a). The scattering geometry is a reference beam backscatter geometry with momentum transfer of the scattering in the radial direction perpendicular to the cylinder axis. The incident laser power was 100mW of 488.0nm blue light. The beam was spatially filtered just prior to entering the apparatus to provide uniform phase across the beam diameter. Light was collected over approximately one coherence solid angle from a measuring control volume which is actually the intersection of a Gaussian profile and an Airy function. However, we can get a reasonable estimate of its dimensions from (3.26)

$$\Delta x = 32\mu m \qquad \Delta y = 31\mu m \qquad \Delta z = 155\ m \qquad (4.1)$$

full width at 1/e intensity. With these dimensions the number of particles simultaneously in the probe volume is 100 and 200 for the two concentrations studied so that the condition for a Gaussian scatered field is always satisfied.

The collected light was beat with a reference beam on the photocathode of a photomultiplier tube. Figure 4.1(b) shows the signal processing and data analysis of the resulting photocurrent. The photocurrent was AC coupled to an amplifier and bandpass filter, then clipped and counted for a fixed time interval with the count transferred to a PDP-8/E minicomputer at the end of the sampling interval. In this this way the frequency of the Doppler signal(and thus the fluid velocity) was simultaneously measured, digitized and stored as a time history in sequential

Figure 4.1

Schematic diagram of the laser Doppler velocimetry system. (a) The optical system. (b) Digital data acquisition and analysis electronics.

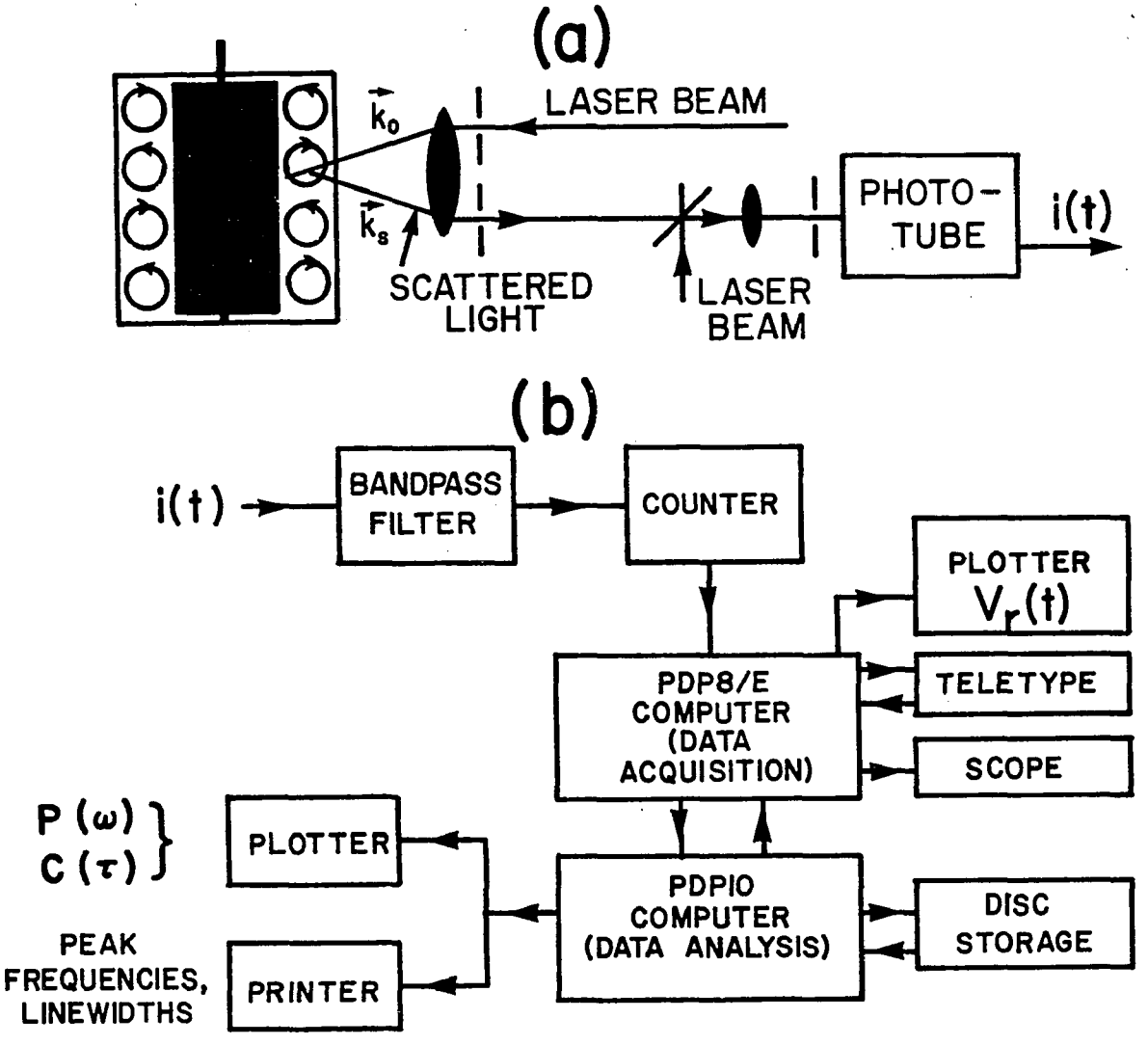
(a)
LASER BEAM
$\vec{k}_o$
$\vec{k}_s$
SCATTERED LIGHT
LASER BEAM
PHOTO-TUBE
i(t)
(b)
i(t)
BANDPASS FILTER
COUNTER
PLOTTER $V_r(t)$
PDP8/E COMPUTER (DATA ACQUISITION)
TELETYPE
SCOPE
P (ω)
C (τ)
PLOTTER
PEAK FREQUENCIES, LINEWIDTHS
PRINTER
PDPIO COMPUTER (DATA ANALYSIS)
DISC STORAGE

locations of the computers memory. The accumulated time history was then transferred by a 4800 baud asynchronous serial receive-transmit interface to the PDP-10 mainframe computer.

In the PDP-10 the power spectral density of the velocity was constructed from the squared modulus of the Fast-Fourier Transform of the velocity time record. The GEO[2] window was applied to the resulting spectrum to suppress leakage and smootning was employed to make the resulting spectral estimate statistically consistent. A record length of 8192 samples gives a frequency resolution of 0.07%(half-width at half-maximum). The theoretical estimate of the resolution has been verified by evaluating a pure sine wave with the full 36-bit accuracy of the PDP-10 and fixing the values to 12 bit integers for 8,192 values of the argument. This program also shows that digitizing noise is at least three orders of magnitude smaller than other noise sources. Figure 4.2(a) shows an unsmoothed plot of a fluid mode whose width is not resolved below the instrument width.

One of the drawbacks of the multichannel frequency counting scheme which results from estimating and digitizing the Doppler frequency in the same step is that aliases are difficult to control. We have found it adequate for our purposes to take spectra with two different sampling times and use the comparison to identify the aliases. The aliases

Figure 4.2

Segments of a velocity power spectrum computed from a velocity record at $R/R_c = 5.7$. The dimensionless frequency is in units of the cylinder frequency and the full spectrum extends from $\omega = 0$ to 2. (a) The solid curve is a high resolution plot with no smoothing; the spectral line is the fundamental frequency component corresponding to the azimuthal waves. The spectrum for a pure sine wave with the same center frequency is shown by the dashed curve (see text). The lineshape and linewidth [full-width at half-maximum (FWHM)] of the fluid spectral component is the same as that of the pure sine wave. (b) The spectral component ω_1 at $\omega = 1.380$ has harmonics $2\omega_1$, $3\omega_1$, etc. which lie beyond the spectral range sampled, $\omega = 0$ to 2. These higher frequency components appear as "aliases" folded into the $\omega = 0$ to 2 spectrum. For example, the component A on the left is at $2\omega_N - 2\omega_1 = 1.240$, where $\omega_N = 2.000$ is the Nyquist frequency; the component A on the right is at $4\omega_1 - 2\omega_N = 1.520$.

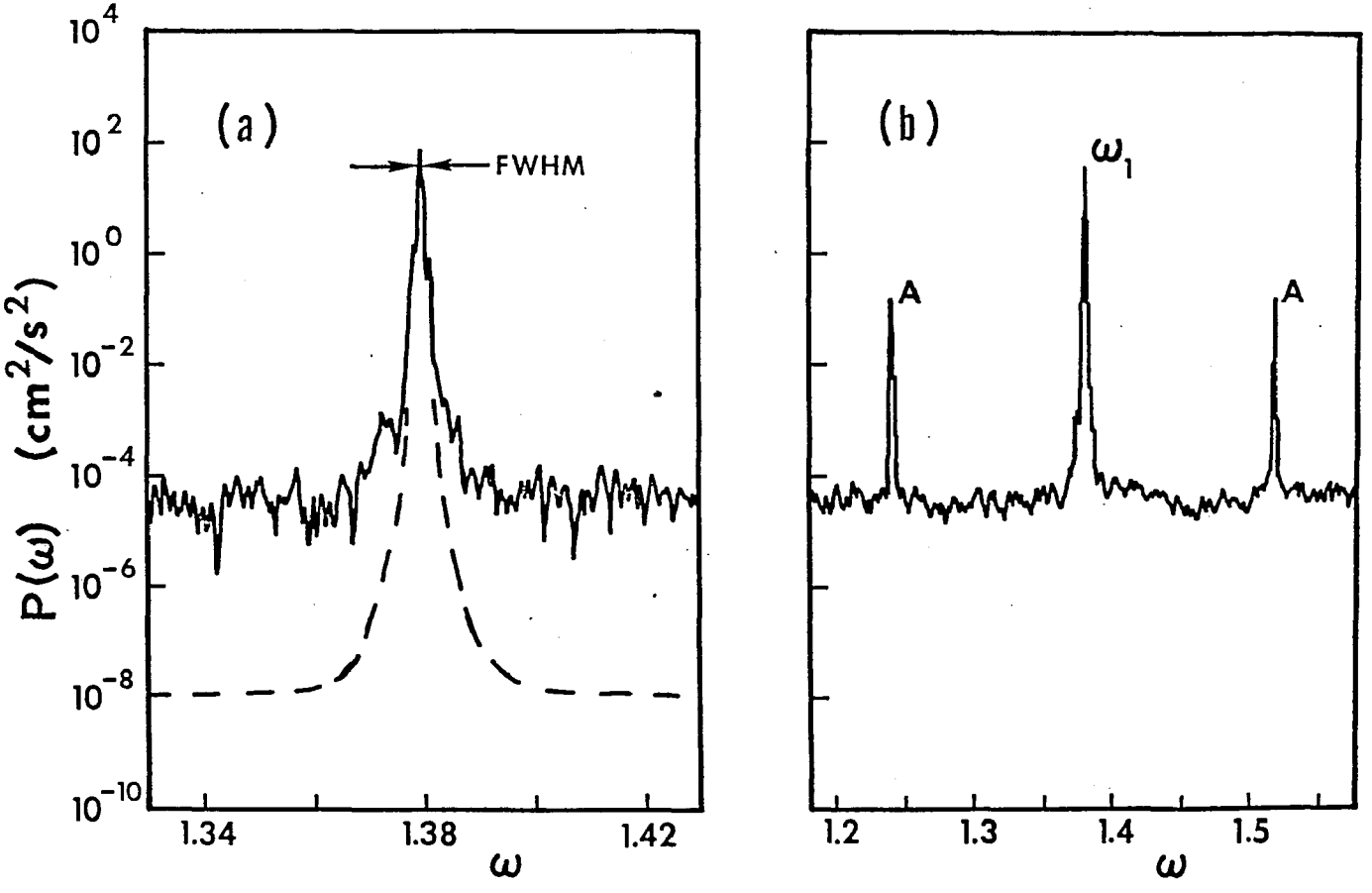
(a)
FWHM
10^4
10^2
10^0
10^{-2}
10^{-4}
10^{-6}
10^{-8}
10^{-10}
P(ω) (cm²/s²)
1.34
1.38
1.42
ω
(b)
ω1
A
A
1.2
1.3
1.4
1.5
ω

are identified in Figure 4.2(b). A relatively small number of harmonics alias into the region of interest due to the fact that accumulating the counts over the duration of a sampling interval is an integrated determination of the frequency which gives the instrument a low pass frequency characteristic with a cutoff frequency of $f = 1/2\Delta t$, where Δt is the sampling time.

Photographs are made by seeding the flow with Kalliroscope[3] AQ1000 rheoscopic liquid. Full cell pictures are taken on 4x5 Tri-X Pan Professional film with small aperture to provide depth of field. A measured exposure time of 50 μs provided by dual electronic flashes freezes the motion to within half the resolving power of the film. The prints are made on Kodak F-4 Azo paper developed in normal Kodak Dektol for 1 1/2 minutes. The same flow cell, temperature control and motor drive are used for both photographic and Laser Doppler measurements.

References for Chapter IV

1. Einstein, A. 1906
cited in Landau, L. and Lifshitz, E.M. 1959
Fluid Mechanics, Reading Mass.: Academic Press

2. Otnes, R.K. and Enochsen, L. 1972 Digital Time Series Analysis. New York: Wiley.

3. Kalliroscope Corp.,Cambridge, Massachusetts.

5. Results

5.1. Principal results

We have studied the radial component of the local fluid velocity at the gap center and axial center of the cell as a function of time over a wide range of Reynolds number. Our results for the frequency of the wavy vortices ω_1 agree with those of Coles[1] to within his experimental accuracy. However, with the high resolution available with long data records we have been able to determine that the ω_1 frequency depends on the axial wavenumber. The frequency also depends on the azimuthal wavenumber, but these changes are large and were previously known. The results presented in the remainder of this subsection will be for the state with 17 axial waves and 4 azimuthal waves (p/m=17/4) which is the state we have studied most extensively to date. The justification for this and results for other states will be presented later.

Figure 5.1 shows velocity fluctuation power spectra representative of the range of Reynolds numbers between 5.4 and 40 over which the state p/m=17/4 is known to be stable, and Figure 5.2 shows photographs of the corresponding visualizations. Figure 5.1(a) shows the spectrum at R/Rc=9.84 with only the ω_1 frequency. Figure 5.2(a) shows the flow at this Reynolds number. Its major features are the waves on the vortex boundaries with a phase angle between the inflow and outflow boundaries and a relative absence of

Figure 5.1

The time-dependence of the radial velocity component and the corresponding velocity fluctuation power spectra for a flow in a concentric cylinder system with specifications as given in the text. The corresponding photographs of the flow are shown in figure 5.2. These data were obtained for water at 27.5 °C except (g) which was obtained at 60 °C. In terms of the dimensionless time t and frequency of the graphs (see text) the time in seconds is given by $4.328t/(R/R_c)$ and the angular frequency in radians/second by $1.452(R/R_c)$, except for (g) where the times (frequencies) are larger (smaller) by a factor of 1.71 because of the smaller viscosity at the higher temperature. The smaller viscosity is the main reason that the velocities in (g) are smaller than in (f) or (h).

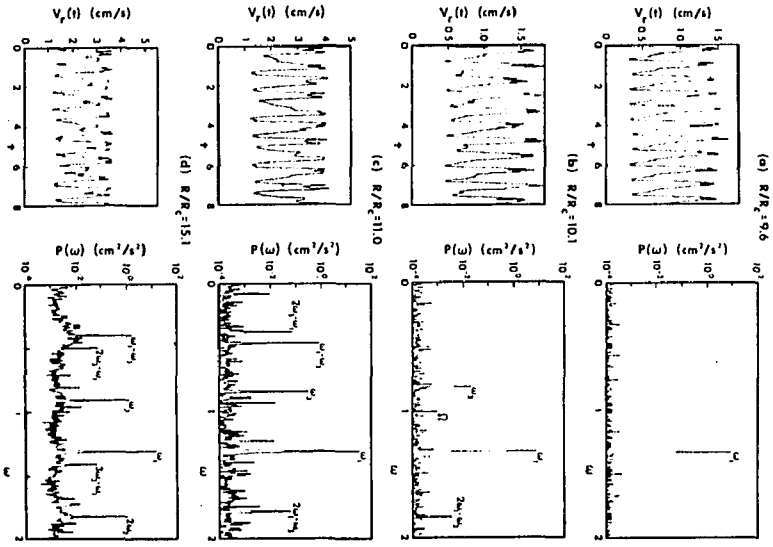
V_r(t) (cm/s)
P(ω) (cm²/s²)
(a) R/R_c=9.6
(b) R/R_c=10.1
(c) R/R_c=11.0
(d) R/R_c=15.1

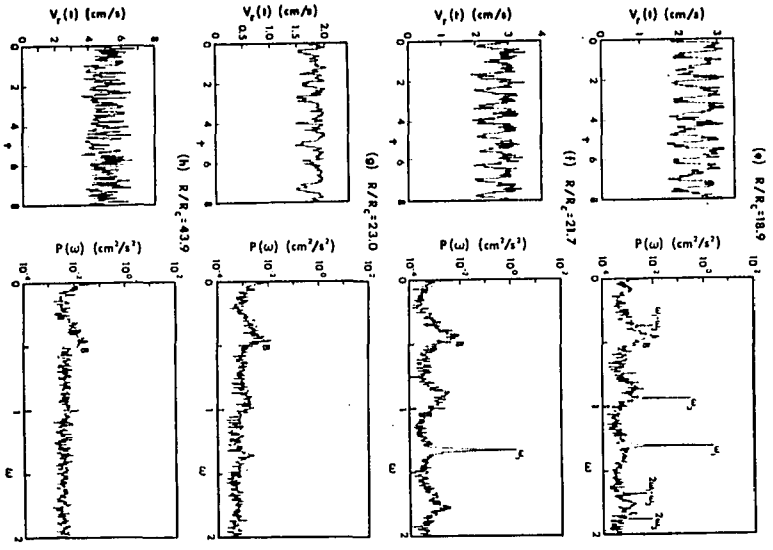
V_r(t) (cm/s)
P(ω) (cm²/s²)
(e) R/R_c=18.9
(f) R/R_c=21.7
(g) R/R_c=23.0
(h) R/R_c=43.9

Figure 5.2

Photographs of the flow corresponding to the velocity graphs and power spectra in figure 5.1. The relative Reynolds numbers R/R_c are: (a) 9.5, (b) 10.5, (c) 11.0, (d) 15.0, (e) 19.0, (f) 21.5, (g) 23.0, (h) 43.3. There are 17 axial vortices and 4 azimuthal waves except in (g) and (h) where the waves have disappeared.

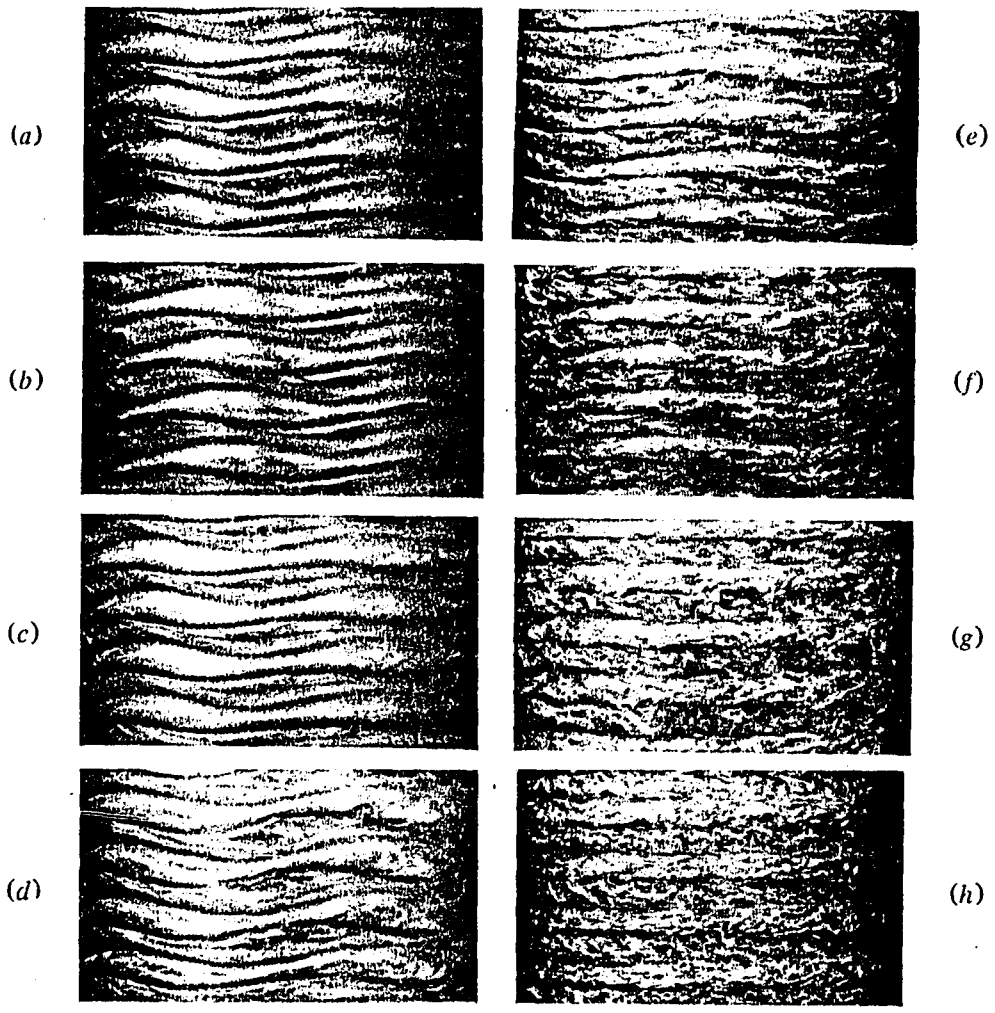
(a)
(b)
(c)
(d)
(e)
(f)
(g)
(h)

small scale structure. In this case the two types of data are simply related. The presence of ω_1 in the velocity power spectrum is due to the propagation of the waves of the vortex boundaries past the probe volume.

We have also found that within the wavy vortex regime there is a range of Reynolds numbers in which a second frequency exists which we have called ω_3 for historical reasons to be discussed later. This mode appears sharply at a relative Reynolds number (R/R_c) of 10.06 as shown in Figure 5.1(b). After its onset this mode grows in amplitude, reaches a maximum, and declines until it dissappears at a relative Reynolds number of 19.3 (Figures 5.1(c)-5.1(g)). This line also has an intrinsic width less than our instrumental resolution. We have been unable to unequivocally identify a feature of the photographs that could lead to such a frequency in the spectra (Figures 5.2(c)-5.2(g)). However, the amplitude of ω_3 is typically two or more orders of magnitude smaller than ω_1 in the vector component studied. Unless its amplitude is appreciably larger in another coordinate direction, it should be difficult to see. Some of the possibilities will be examined in the discussion section.

Within the regime in which both ω_1 and ω_3 are present a third spectral feature appears, but unlike the others this feature has measureable width (Figure 5.1(d)). We have called this feature B because of its broadness. This

broadness makes the exact Reynolds number of its appearance more difficult to determine. B grows in amplitude as the Reynolds number is increased until it eventually dominates the spectrum Figure 5.1(j).

At a relative Reynolds number higher than the disappearance of ω_3 with B quite prominent, there is a sharp change in the nature of ω_1. At R/Rc=21.9 ω_1 acquires a measurable width and decreases in amplitude. This can be seen by comparing figures 5.1(h) and 5.1(i). Note that because of the logarithmic scale the half power point is very close to the tip of the peak. At slightly higher Reynolds number (23) ω_1 cannot be resolved beneath the harmonics of the B mode which now is two orders of magnitude larger in amplitude than its initial appearance. This is reflected in the visualization results at this Reynolds number as a disappearance of periodic waves on the vortex boundaries as well as a rich small scale structure. Figure 5.3 shows the two extremes of velocity power spectra (a) showing a Reynolds number near the lowest for which the 17/4 cell state is stable and (b) being near the highest studied.

A summary plot of the frequencies of the observed modes as a function of the relative Reynolds number is shown in Figure 5.4. Tnroughout most of the range ω_1 is fairly constant with an increase at both extremes, the upturn at the high end being more dramatic. Where it exists ω_3 is

Figure 5.3

Power spectra of the radial velocity component for the flow between concentric cylinders in the system described in the text. The spectrum in (a) corresponds to the flow pictured in figure 2.3(b) and (b) corresponds to that pictured in figure 5.1(h).

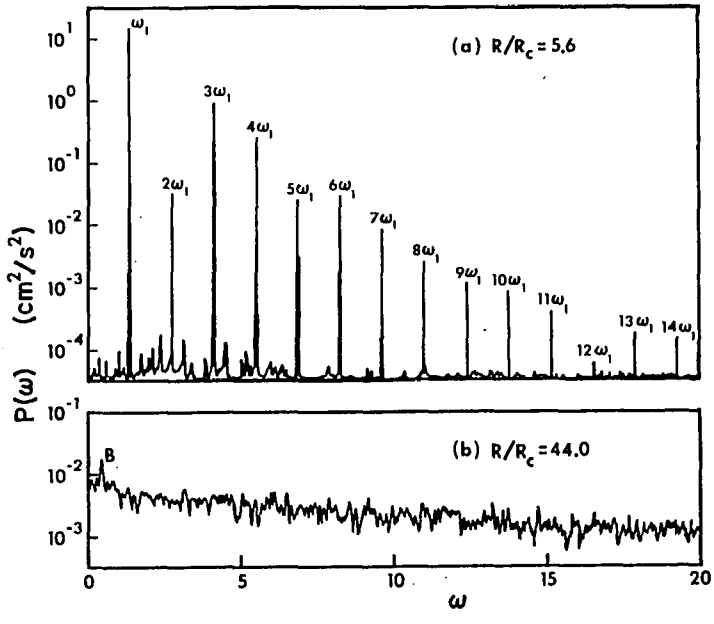
(a) R/R$_c$ = 5.6
(b) R/R$_c$ = 44.0
B
P(ω) (cm^2/s^2)
ω
ω_1
$2\omega_1$
$3\omega_1$
$4\omega_1$
$5\omega_1$
$6\omega_1$
$7\omega_1$
$8\omega_1$
$9\omega_1$
$10\omega_1$
$11\omega_1$
$12\omega_1$
$13\omega_1$
$14\omega_1$
10^1
10^0
10^{-1}
10^{-2}
10^{-3}
10^{-4}
0
5
10
15
20

Figure 5.4

The fundamental frequency components observed in the power spectra of the radial velocity component for a flow with 17 vortices and 4 waves in a system with specifications given in table 2 of chapter 4. No sharp spectral components were observed above $R/R_c = 21.9$. The triangular points and vertical bars indicate respectively, the center frequency and linewidth (FWHM) of the broad component B; the horizontal bar is its average center frequency.

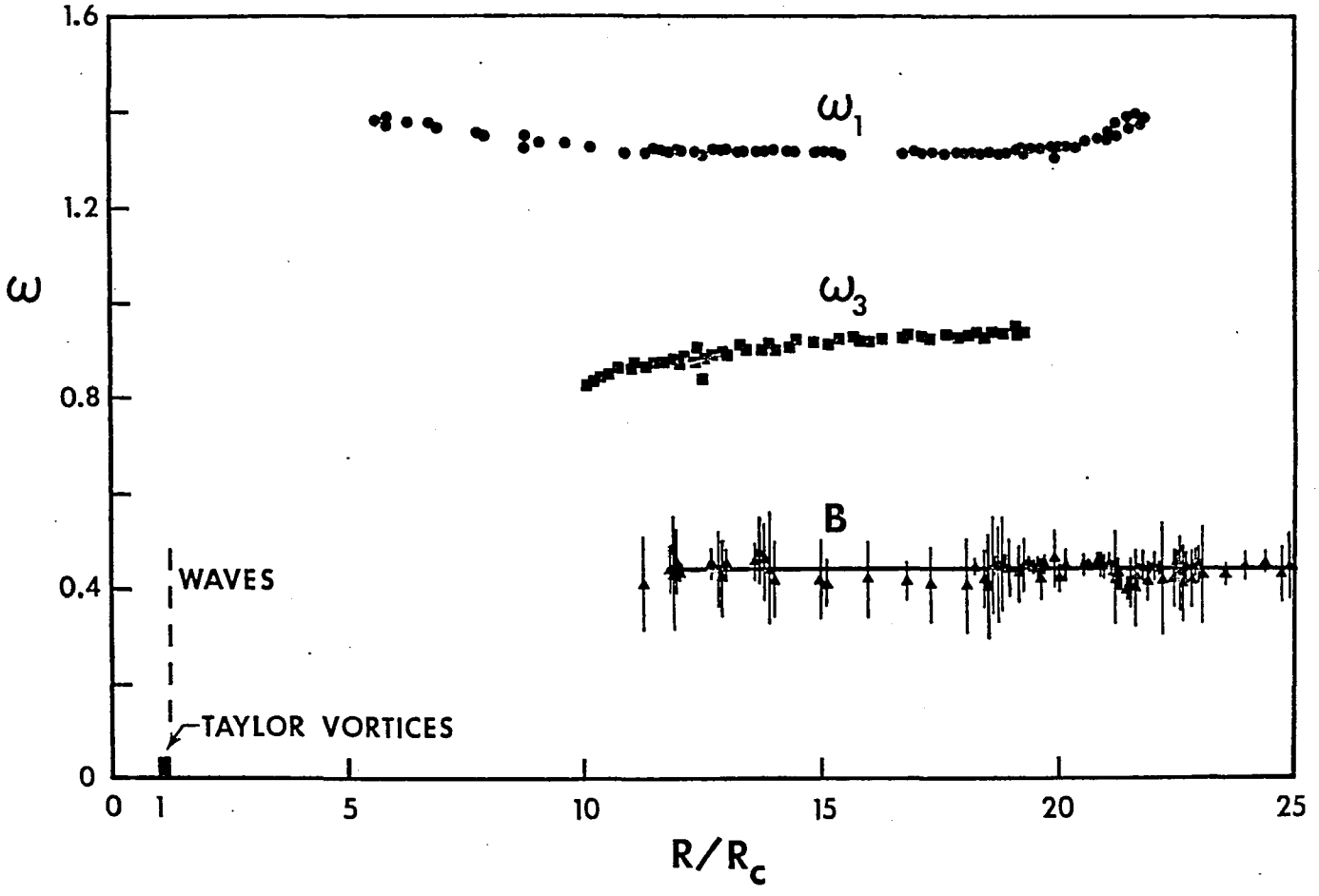
1.6
1.2
0.8
0.4
0
ω
ω_1
ω_3
B
WAVES
TAYLOR VORTICES
0
1
5
10
15
20
25
R/R_c

montonically increasing. The broad mode B due to its complex shape is difficult to assign a precise frequency, but to the limit of accuracy it appears to be constant in frequency throughout the interval in which it is detected. For the same reason the Reynolds number at which B first appears is difficult to determine, but it is in the interval (12,14).

Figure 5.5 shows the ratio ω_3/ω_1 as a function of Reynolds number. We note that the ratio 2/3 occurs on the lower edge of the range in which B first appears. There is also the suggestion of frequency locking, but the spread in the data forces us to regard this as merely suggestive. Figure 5.6 shows the difference frequency $\omega_1 - \omega_3$ as a function of Reynolds number with the center frequency of the B mode indicated. Again the coincidence is at the lower edge of the region where B first appears, but the width of that interval bars certainty.

Figure 5.5

The dependence of ω_3/ω_1 on Reynolds number in the regime where ω_3 was observed. The significance of $\omega_3/\omega_1 = 2/3$ is discussed in chapter 6.

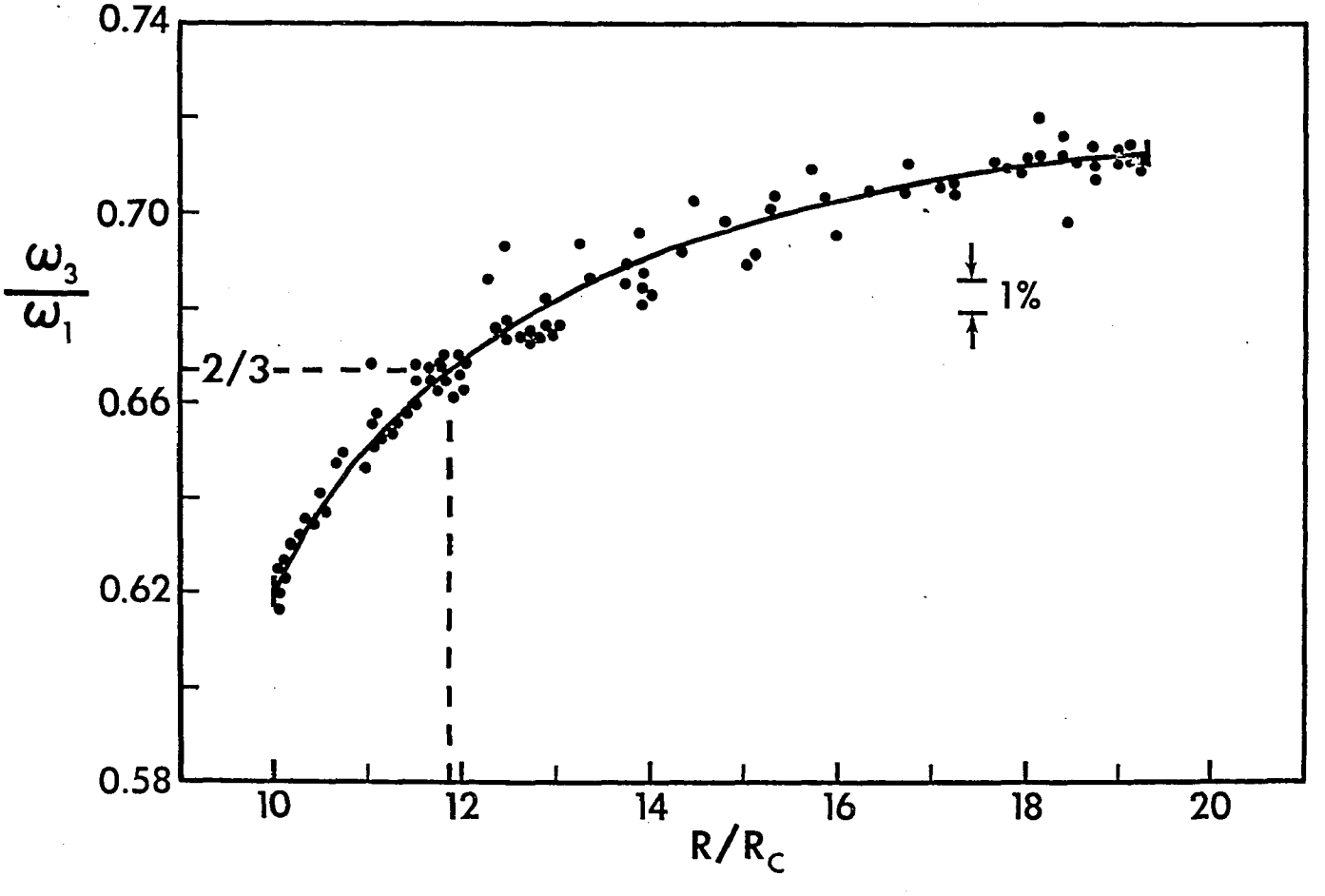
0.74
0.70
0.66
0.62
0.58
$\frac{\omega_3}{\omega_1}$
2/3
1%
10
12
14
16
18
20
R/R_C

Figure 5.6

This graph supports the conjecture that the broadband component B is excited by the component at $\omega_1 - \omega_3$, since B is first observed at $R/R_c \simeq 12$.

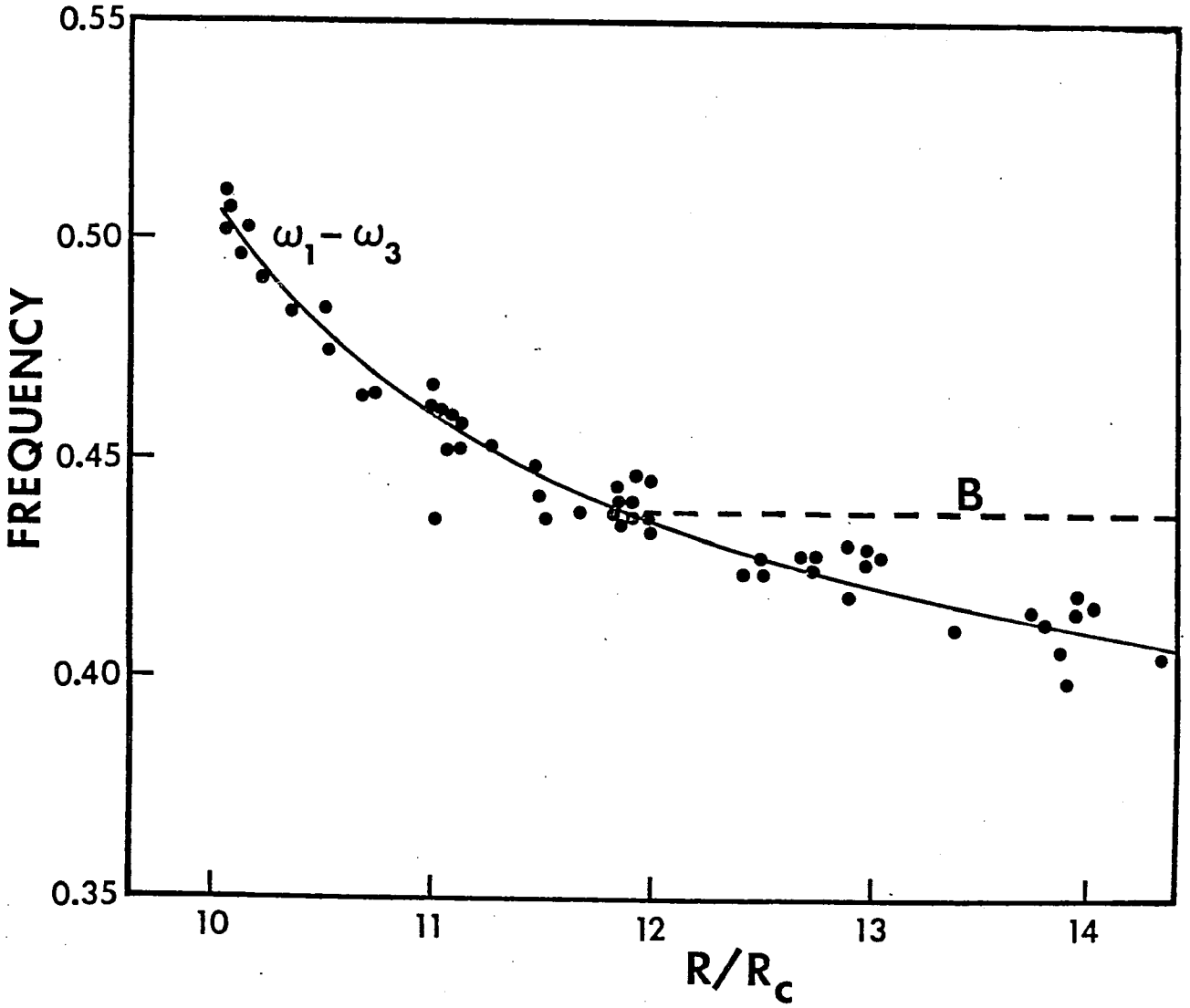
0.55
0.50
0.45
0.40
0.35
FREQUENCY
$\omega_1 - \omega_3$
B
10
11
12
13
14
R/R_c

5.2. Other results

In some of the runs we have seen a very low frequency mode which we have called ω_2 because it first appears, if at all, at Reynolds numbers intermediate between the appearance of ω_1 and the appearance of ω_3. This feature is not reproducible from run to run, but appears to be fairly reliably produced by rapid starts to relative Reynolds numbers of approximately 8 to 12. When it appears it may last for only a few minutes or it may last as long as two hours. A plot of ω_2 as a function of Reynolds number is shown in Figure 5.7. The ω_2 frequency decreases monotonically to zero with increasing Reynolds number.

We have also confirmed the appearance of subcritical shadow vortices initially reported by Cole[2]. We have observed the onset of the wavy vortex state and have found it to be in reasonable agreement with the theoretical prediction of DiPrima, Stuart, and Davy [3] with respect to the critical Reynolds number for the transition. However, their calculation suggests that the m=1 mode should be the first to go unstable while we observe m=5 to be the most unstable.

In addition to the studies on the 17/4 state mentioned in the previous subsection we have also studied the 15/4 state. Figure 5.8 is a comparison of the ω_1 frequencies for these two states. Either state, once achieved, is stable as the Reynolds number is changed quasistatically between

Figure 5.7

These data illustrate the characteristics of the transient mode ω_2 . (a) A portion of a velocity record obtained at $R/R_c = 13.0$. The times T_1 and T_2 are respectively the periods of the components with frequencies ω_1 and ω_2 . (b) The power spectrum corresponding to the velocity record in (a). (c) Dependence of ω_2 on Reynolds number.

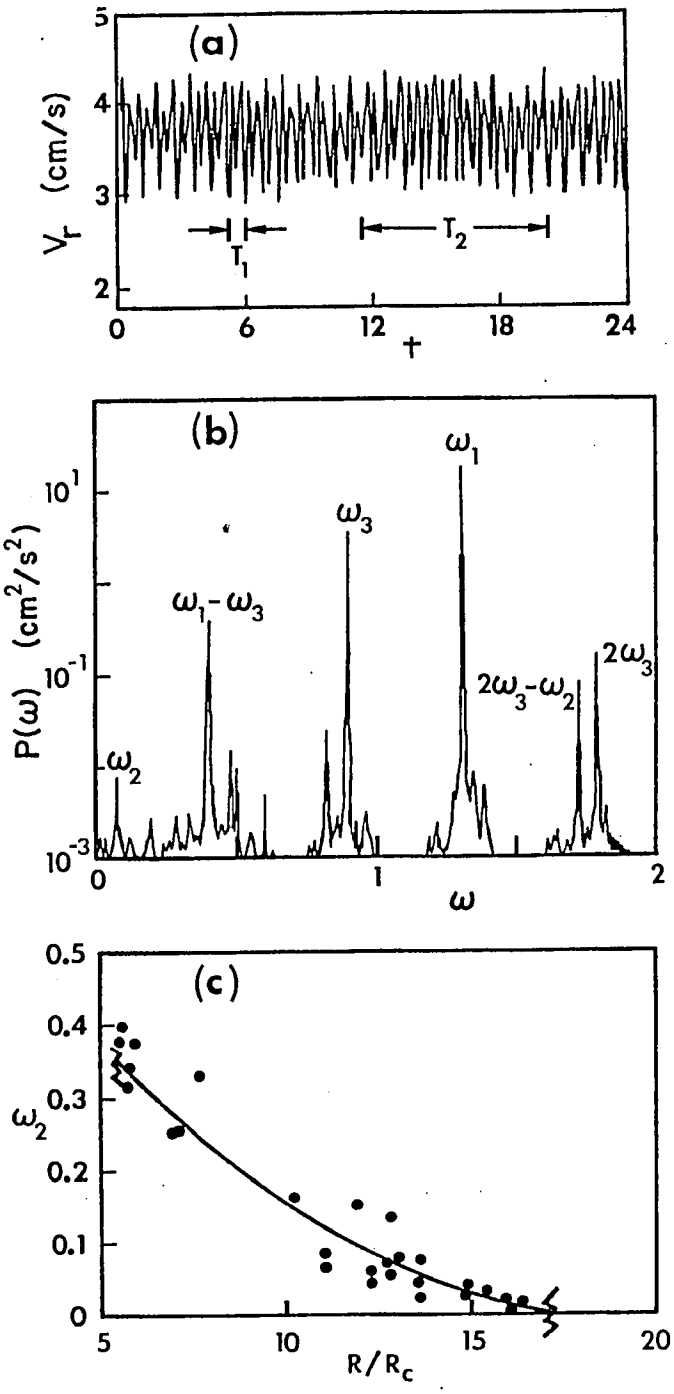
(a)
V_r (cm/s)
T_1
T_2
t
(b)
$P(\omega)$ (cm^2/s^2)
ω_1
ω_3
$\omega_1-\omega_3$
$2\omega_3-\omega_2$
$2\omega_3$
ω_2
ω
(c)
ω_2
R/R_c

Figure 5.8

A comparison of the ω_1 frequency as a function of Reynolds number for the 17 cell state and the 15 state. Shown in the upper left hand corner is a scale indicating a frequency difference of 1%.

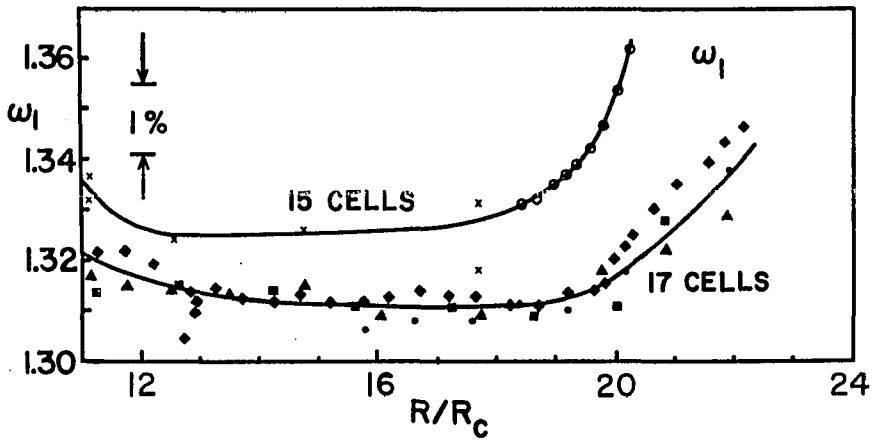
1.36
1.34
1.32
1.30
ω1
1%
15 CELLS
17 CELLS
ω1
12
16
20
24
R/Rc

moderate values (5.4) through the disappearance (19.5) and somewhat above (45) in either direction. These results are reproducible independent of how the state is achieved. Visualization studies with different cell fillings show that this stability-lack of transitions to other states-is a property of relatively short cell fillings. Longer cells have more accessible states and more transitions between them. Figure 5.9 shows the transition between the m=4 and m=5 states as the Reynolds number is decreased. The implications of this will be explored in the next section..

Figure 5.9

The discontinuous variation of the azimuthal wave frequency when the number of azimuthal waves changes from 4 to 5 as the Reynolds number is decreased through $R/R_c = 5.4$ for the state with 17 axial vortices. The wave frequency ω_1 jumps from 1.38 to (5/4) x 1.38 = 1.73.

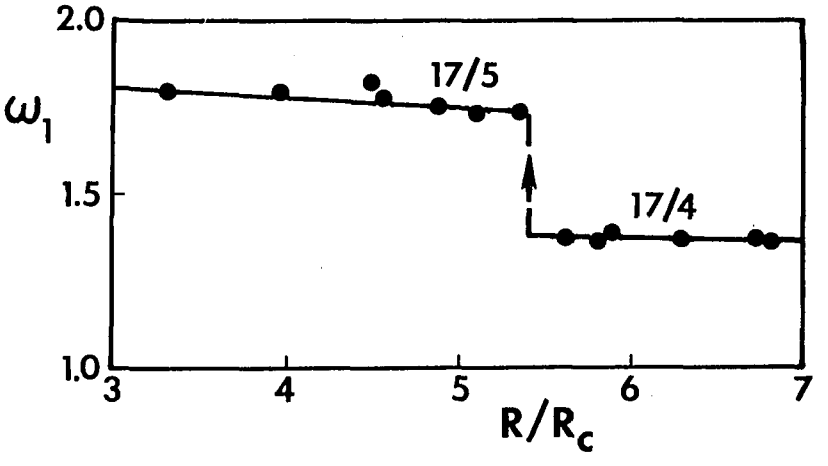
2.0
1.5
1.0
ω_1
17/5
17/4
3
4
5
6
7
R/R_c

References for Chapter V

1. Coles D. 1965 Transition in circular Couette flow. J. Fluid Mech. 21, 385-425.

2. Cole, J.A. 1976 Taylor-vortex instability and annulus-length effects. J. Fluid Mech. 75, 1-15.

3. Davey, A., DiPrima, R.C., and Stuart, J.T. 1968 On the instability of Taylor vortices. J. Fluid Mech. 31, 17-52.

6. Discussion

All the results presented here support the central conclusion of Gollub and Swinney[1] that the Landau picture of the transition to turbulence is not correct for this system. The question posed by Hopf[2] about how the nonlinearity of his model compares to that of the hydrodynamic case, appears to have an answer. They are sufficiently different to lead to qualitatively different behavior. After expending the effort to determine this fact experimentally, it is easy to convince ourselves that this answer is not surprising. Nonlinearity enters the Hopf model only through the convolution integrals over a period of the fundamental of the Fourier series The result of this is that modes of different wavevector do not interact. The progression of instabilities is a sequence of k-modes independently becoming unstable. In the hydrodynamic case, however, the nonlinear terms couple modes of different wavevector so that the stability of any given mode depends on the strength of the coupling to other modes and their stability.

There remain the questions of whether the Couette flow system is an example of either the Lorenz[3] attractor or an attractor of the type discussed by Ruelle-Takens[4]. In terms of the number of time-dependent instabilities preceding the onset of chaos, it appears on the surface that the system cannot be a Lorenz attractor but may be a Ruelle-Takens attractor. Earlier, however, when the number of

time-dependent instabilities was believed to be greater than it now appears, Ruelle[5] suggested that the time-dependence of of ω_1 might be transformed away in the appropriate rotating frame of reference. If this is true then the possibility that choas in Taylor vortex flow is a Lorenz attractor is reopened. However, photographic results which suggest this are insensitive to effects near the inner and outer walls where one would expect things to change rapidly. LDV measurements are needed on this point. One might take the reasonable success of the theory of DiPrima, Davey, and Stuart[6] as indication of the rigid rotation of but the question of behavior near the walls is left somewhat open by the neglect of higher order terms which one would need to characterize a thin layer accurately. Finally, to add a reservation about our reservations, it is not clear how exact the cancellation of the time-dependence by the coordinate transform must be.

The aim of accurate measurement of the frequencies of the fluid modes and the Reynolds number at which they appear is to attempt to identify if possible what kind of instability ultimately leads to the unpredictable behaviour in the flow. One hope is to find a match with known instability modes. If the center frequency of B can be accurately determined, one can then examine whether that Reynolds number is the first occasion where $\omega_1 - \omega_3 = B$. This would suggest that the appearance of B was due to ω_1 and ω_2 coupling nonlinearly to a mode which remains unexcited until

resonance is reached.

It has also been suggested by Bowen[7] that the first appearance of B might occur when the ratio $\omega_3/\omega_1 = 2/3$. His argument is based on the observation that the trajectory of the system in phase space changes topological type when the frequencies become commensurate. When the frequencies are incommensurate the phase trajectory fills the surface of a torus, whereas when the frequencies become commensurate the trajectory collapses to a single closed curve on the torus. While the rational numbers are dense in the reals the sentiment that small integer ratios should be important leads one to the choice $\omega_3/\omega_1 = 2/3$ as the ratio of the smallest integers in the range over which is observed. Ruelle and Takens have also suggested the importance of small integer ratios but suggest a different effect , namely that once the frequencies become commensurate they should remain so over a finite interval of Reynolds number. Figure 5.5 shows a plot of ω_3/ω_1 over the range of Reynolds number for which ω_3 exists. While there are irregularities in data near the ratio 2/3 and the occurance of B is within an interval of Reynolds number which contains this ratio, neither of these observations can be considered statistically significant.

The stability of a state under quasistatic change of Reynolds number suggests that while different states may be nearly degenerate in energy, they are separated by a barrier

of reasonable height, making it unlikely that the non-uniqueness of state is related to the dynamics of the transition. The reproducibility of the results further supports this assertion. We assert that the problem of the dependence of the behavior of this system on the Reynolds number history can be effectively factored into two separate problems. The first being the dependence of the state on the Reynolds number history and the second being the transition to turbulence under quasistatic changes in Reynolds number of a given state.

We suggest an explanation of the increasing non-uniqueness of the observed flows with increasing aspect ratio which is an extension of the work of Benjamin mentioned earlier. He showed that the presence of boundaries lifts the degeneracy with respect to reversal of the velocities and that the resulting separation of otherwise degenerate states increases as one goes to smaller aspect ratios. We suggest that the non-uniqueness of the axial wavenumber arises from a lifting of the periodic translational symmetry of the infinite cylinder problem. The increasing separation of states with decreasing aspect ratio indicates that the energy barrier between adjacent states is larger for short cylinders resulting in fewer states being accessible with the available energy.

We believe that the appearance of the shadow vortices in the Couette flow regime might have a relatively simple

explanation. As mentioned earlier a solid boundary introduces an inward radial component to the flow near the boundary and a free surface introduces an outward component. The linear stability analysis for this regime shows that the imaginary frequency of the vortex mode passes continuously from negative to positive values as the Reynolds number passes through the critical number from below. Thus for slightly subcritical Reynolds number the vortex mode is only weakly damped. Since the radial forces at the boundaries share the symmetry of the vortex mode they can excite it. Since the excitation occurs in a thin layer near the boundary the vortex amplitude should be greatest there decreasing inward in the z-direction. Close to the critical Reynolds number this decay should be exponential.

Finally, we would like to draw attention to the very close correspondance between the Reynolds number at which the m=4 to m=5 transition is observed and the appearance of the transient mode ω_2 in the 17 cell state. This suggests that this mode may be related to a mode hopping frequency between the two states. This transition between states probably displays hystersis and the mode may be easier to excite in the overlap region even though it exists outside that region. However, the mechanism would have to be able to explain why once excited, the mode remains excited when the Reynolds number is increased.

References for Chapter 6

1. Gollub, J.P. and Swinney, H.L. 1975 Onset of turbulence in a rotating fluid. Phys. Rev. Lett. 35, 937-930.

2. Hopf, E. 1948 A mathematical example displaying features of turbulence. Comm. Pure Appl. Math., 1,303.

3. Ruelle, D. 1976 The Lorenz attractor and the problem of turbulence. Quantum Dynamics: Models and Mathematics. Streit, L., ed., New York Springer-Verlag.

4. Ruelle, D. and Takens, F. 1971 On the nature of turbulence. Commun. Math. Phys. 20, 167-192.

5. Ruelle, D. private communication.

6. Davey, A., DiPrima, R.C., and Stuart, J.T. 1968 On the the instability of Taylor vortices. J. Fluid Mech. 49, 529-550.

7. Bowen, R. 1977 A model for Couette flow data, Berkeley Turbulence Seminar, Springer Lecture Notes in Mathematics 615,117-134.

7. Conclusion

We have presented velocity fluctuation power spectra one order of magnitude higher in resolution and three orders of magnitude lower in instrumental noise than previous studies. As a result we have been able to demonstrate the strict time periodicity of wavy vortex flow to a new degree of precision. We have also provided the first definitive demonstration of a quasi-periodic fluid flow. We have shown that the question of non-uniqueness of the flow as a function of Reynolds number and the transition to turbulence are separate issues. We have shown that the behavior is similar but distinct in different states.

We have shown that the first appearance of random behaviour occurs after only three bifurcations and that this random element coexists with the periodic components present at lower Reynolds numbers. We have suggested that the appearance of chaos is an instability related to a frequency condition between two periodic components.

We have presented suggestive evidence for the assertion that the appearance of chaos is dynamically related to the coupling between two sharp modes and a third.